Journal of Experimental Botany, Vol. 76, No. 8 pp. 2112–2128, 2025
https://doi.org/10.1093/jxb/eraf017 Advance Access Publication 15 January 2025

RESEARCH PAPER

Kifunensine-sensitive *ADP-ribosylation factor A1E*^{G69R} mutant reveals coordination of protein glycosylation and vesicle transport pathways

Yukihiro Nagashima[1], Vinita Sharma[1], Lea-Franziska Reekers[2], Antje von Schaewen[2], and Hisashi Koiwa[1,3,*]

[1] Vegetable and Fruit Improvement Center and Department of Horticultural Sciences Texas A&M University, College Station, TX 77843, USA
[2] Institut für Biologie und Biotechnologie der Pflanzen, Universität Münster, D-48149 Münster, Germany
[3] Molecular and Environmental Plant Sciences, Texas A&M University, College Station, TX 77843, USA

* Correspondence: Hisashi.Koiwa@ag.tamu.edu

Received 23 October 2024; Editorial decision 10 January 2025; Accepted 11 January 2025

Editor: Richard Napier, University of Warwick, UK

Abstract

Complex *N*-glycans are asparagine (*N*)-linked branched sugar chains attached to secretory proteins in eukaryotes. They are produced by modification of *N*-linked oligosaccharide structures in the endoplasmic reticulum and Golgi apparatus. Complex *N*-glycans formed in the Golgi apparatus are often assigned specific roles unique to the host organism, with their roles in plants remaining largely unknown. Using inhibitor (kifunensine, KIF) hypersensitivity as read out, we identified Arabidopsis mutants that require complex *N*-glycan modification. Among >100 KIF-sensitive mutants, one showing abnormal secretory organelles and a salt-sensitive phenotype contained a point mutation leading to amino acid replacement (G69R) in ARFA1E, a small Arf1-GTPase family protein presumably involved in vesicular transport. *In vitro* assays showed that the G69R exchange interferes with protein activation. *In vivo*, ARFA1E^{G69R} caused dominant-negative effects, altering the morphology of the endoplasmic reticulum, Golgi apparatus, and *trans*-Golgi network (TGN). Post-Golgi transport (endocytosis/endocytic recycling) of the essential glycoprotein KORRIGAN1, one of the KIF sensitivity targets, is slowed down constitutively as well as under salt stress in the ARFA1E^{G69R} mutant. Because regulated cycling of plasma membrane proteins is required for stress tolerance of the host plants, the ARFA1E^{G69R} mutant established a link between KIF-targeted luminal glycoprotein functions/dynamics and cytosolic regulators of vesicle transport in endosome-/cell wall-associated tolerance mechanisms.

Keywords: ARFA1, cell wall, complex *N*-glycans, kifunensine, root development, small GTPases, vesicle transport.

Abbreviations: ARF, ADP ribosylation factor; ARF-GAP, ARF GTPase-activating protein; ARF-GEF, ARF guanine nucleotide exchange factor; BFA, brefeldin A; BIG5, brefeldin A-inhibited guanine nucleotide exchange factor 5; BiP, binding protein; CGL1, complex glycan-less 1; EE, early endosome; EMS, ethyl methanesulfonate; ER, endoplasmic reticulum; KIF, kifunensine; KOR1, KORRIGAN1; MNS, mannosidase; MS, Murashige and Skoog; NGS, next-generation sequencing; PHT, phosphate transporter; PI4K, phosphatidylinositol 4-kinase; PLD1, phospholipase D1; PRC, procuste; RSW, RADIALLY SWOLLEN; SYP61, SYNTAXIN OF PLANT61; SOS, salt overly sensitive; TGN, *trans*-Golgi network; VHA-A3-L*ssm*OR, VACUOLAR PROTON ATPASE-A3-long stokes shift *monomeric* Orange; WT, wild type; XYLT, xylosyltransferase

Introduction

N-Glycosylation of soluble and membrane-bound secretory proteins is an essential post-translational modification in eukaryotic cells, including plants (Nagashima *et al.*, 2018). In the endoplasmic reticulum (ER), pre-assembled core oligosaccharides are first attached co-translationally to asparagine residues in the N-X-S/T sequon (X stands for any amino acid, except proline) of nascent polypeptide chains upon import. The *N*-linked core glycans then undergo rounds of trimming by two α-glucosidases [I and II, equivalent to RADIALLY SWOLLEN3 (RSW3)] and α-mannosidase I (MNS3 in *Arabidopsis thaliana*) in the ER lumen. This process is coupled with protein folding assistance by calnexin, calreticulin, and other lectin chaperones, which recognize terminal glucose residues on the core *N*-glycans. When initial folding fails, UDP-glucose:glycoprotein glucosyltransferase (UGGT) restores glucose decoration on the *N*-glycan A branch to repeat the folding attempt. Once correctly folded, glycoproteins with trimmed *N*-glycans exit the ER and are transported to the Golgi apparatus, whereas proteins that fail to fold correctly after multiple rounds of folding attempts are removed by the ER-associated degradation (ERAD) pathway, with α-mannosidase II (OS9; Hüttner *et al.*, 2012) initiating the ERAD process, and two ER-resident α-mannosidase I isoforms (MNS4 and MNS5; Hüttner *et al.*, 2014) not involved in regular *N*-glycan processing. In the Golgi apparatus, further trimming of the *N*-glycan structures occurs by Golgi α-mannosidase I isoforms (MNS3, then MNS1 and MNS2), followed by maturation reactions catalyzed by *N*-acetylglucosaminyltransferase I (GNTI/CGL1, COMPLEX GLYCAN-LESS1), Golgi α-mannosidase II (GMII/HGL1, HYBRID GLYCOSYLATION1), and a suite of glycosyltransferases to produce various forms of plant-specific complex *N*-glycans (reviewed in Nagashima *et al.*, 2018).

In contrast to the well-established biosynthesis of *N*-glycans and their ubiquitous role in protein folding within the ER, the biological functions of individual plant *N*-glycans, and the significance of their maturation to complex *N*-glycans, remain elusive. Knockout mutations affecting early *N*-glycosylation and modification reactions within the ER resulted in gamete or zygote lethality. Three α-mannosidase I isoforms were shown to localize to the interface between the ER and *cis*-Golgi cisternae (Schoberer *et al.*, 2019) and, when their activities were blocked, either by knockout mutations (*mns1,2,3* triple) or by the α-mannosidase I-specific inhibitor kifunensine (KIF) (Elbein *et al.*, 1991), the host plants suffered severe inhibition of root growth and radial tip swelling in Arabidopsis. This is likely to be caused by compromised modification of the B and C branches present in plant *N*-glycans (Veit *et al.*, 2018). In contrast to plants with α-mannosidase I defects, those with mutations in the downstream Golgi *N*-glycan maturation pathway, such as *cgl1*, *hgl1*, or *fucTa fucTb xylT* (*fxT*) triple mutant plants, have not been associated with any apparent phenotypes under normal growth conditions (von Schaewen *et al.*, 1993; Strasser *et al.*, 2006; Kang *et al.*, 2008). Therefore, mannose trimming appears more important for root formation than the derivatization of trimmed oligomannosidic glycans to complex *N*-glycans. However, the *cgl1* and downstream mutations led to salt hypersensitivity in Arabidopsis (Kang *et al.*, 2008), and a homologous defect caused lethality in rice (Fanata *et al.*, 2013). In general, the severity of the salt sensitivity phenotype increases when a mutation occurs upstream of the *N*-glycosylation pathway. For example, the *cgl1* phenotype is more severe than the *hgl1* or *fucTa fucTb xylT* triple mutant phenotype. The mechanism of stress sensitivity in these complex *N*-glycan mutants has been, at least in part, attributed to interference with cellulose biosynthesis. Cellulose deficiency has been detected in some *N*-glycosylation mutants. Also reported were strong genetic interactions between complex *N*-glycan defects and mutation in *rsw2/kor1*, coding for the glycoprotein KORRIGAN1 (KOR1) (Kang *et al.*, 2008), which is part of the cellulose biosynthesis machinery (Mansoori *et al.*, 2014; Vain *et al.*, 2014).

KOR1 is a type II membrane protein with endo-1,4-β-D-glucanase activity, carrying eight *N*-glycans on its extracellular catalytic domain (Rips *et al.*, 2014). We previously showed that *N*-glycan decoration is essential for KOR1 to exit from the ER during folding surveillance and also for remaining in the cycle between initial secretion to the plasma membrane and regular endocytosis to the *trans*-Golgi network (TGN) (Rips *et al.*, 2014; Nagashima *et al.*, 2020a). By contrast, underglycosylated KOR1 variants accumulated at the tonoplast and were degraded (Rips *et al.*, 2014; Nagashima *et al.*, 2020a). On the other hand, a direct role for complex *N*-glycan maturation on KOR1 for protein function has yet to be determined, as have the global biological functions of the complex *N*-glycan modification pathway in plant cells.

Within the secretory pathway, glycoproteins are transported between linked organelles through intracellular trafficking routes, including COP-II (Golgi anterograde route), COP-I (Golgi retrograde route), and clathrin-coated vesicles that specifically operate in post-Golgi trafficking. Eukaryotic ADP-ribosylation factor (ARF) GTPases mediate the assembly of coat proteins on the vesicle surface during the formation of COP-I and clathrin-coated vesicles (Naramoto *et al.*, 2010; Yorimitsu *et al.*, 2014; Singh *et al.*, 2018). Switching between the GDP- and GTP-binding form of ARFs, by the function of ARF guanine nucleotide-exchange factors (ARF-GEFs) and ARF GTPase-activating proteins (ARF-GAPs), controls the recruitment of ARF1 to target membranes via exposure of a membrane anchor within an N-terminal sequence of ~12 residues. This lipid anchor (*N*-myristoylation of glycine at position 2) is retracted into a surface groove on GDP-bound ARF but becomes exposed for membrane binding upon conformational change on GTP-bound ARF (Randazzo *et al.*, 1995; Goldberg, 1998; Pasqualato *et al.*, 2002). Thus, ARF-GEFs activate ARF

proteins, and the activated, GTP-laden ARFs start the formation of vesicles. Accordingly, ARF activation by a cognate GEF is key to controlling the timing and location of vesicle budding events (Mossessova *et al.*, 2003). In Arabidopsis, 19 ARF/ARF-like genes were found (Vernoud *et al.*, 2003; Gebbie *et al.*, 2005), and a major group (ARF-A type) consists of six members (ARFA1A–ARFA1F) with high (>97%) amino acid similarity (Rui *et al.*, 2022). Furthermore, antisense RNA-mediated simultaneous suppression of several *ARFA1* family members resulted in a slight decrease in cellulose and an increase in soluble sugars, such as rhamnose (Gebbie *et al.*, 2005). Hence, although proteins of the ARFA1 family are important players within the secretory system, the specific mechanisms regulated by different ARFA1 isoform members are not fully understood in plants.

To expand our knowledge about the roles of *N*-glycosylation within the plant secretory system, we conducted a screen for increased sensitivity towards an inhibitor of *N*-glycan modification (KIF). One mutant that was identified carried a novel mutation in *ARFA1E* that is involved in vesicle trafficking. Its KIF hypersensitivity was associated with altered morphology of multiple organelles, including the ER, Golgi stacks, and the TGN, indicating that ARFA1E functions in multiple steps of the secretory pathway. An *in vitro* assay revealed that the mutation impairs GDP–GTP exchange, retaining the mutated ARFA1E^{G69R} protein in an inactive form. Moreover, its dominant-negative effect caused salt sensitivity and alterations in stress-induced protein translocation events in the isolated *ARFA1E^{G69R}* mutant plants, indicating that ARFA1E has an important function in coordinating membrane trafficking under stress, linking luminal glycoprotein biogenesis targeted by KIF and cytoplasmic regulation of membrane protein transport.

Materials and methods

Plant materials

Arabidopsis thaliana var. Columbia (Col-0) and Landsberg erecta (Ler) ecotypes were used in this study. The mutant genotypes *rsw2-1* and *stt3a-2* have been described previously (Lane *et al.*, 2001; Koiwa *et al.*, 2003). The green fluorescent protein (GFP)–KOR1 CFP–SYP61 (cyan fluorescent protein–SYNTAXIN OF PLANTS61) line is described in Rips *et al.* (2014) and the *cgl1-3* T-DNA line in Frank *et al.* (2008). Mutant lines of *COBRA* (*cob-1*), *PROCUSTE1/CESA6/IRX2* (*prc1-1*), *PHOSPHATE TRANSPORTER4;6* (*pht4;6*), *SALT OVERLY SENSITIVE5* (*sos5-1*), and *ARFA1E* (*arfa1e-2* T-DNA line GK-835H10-025700) were obtained from the Arabidopsis Biological Resource Center. Binding protein (BiP)–*m*Cherry and VHA-A3-Lss*m*OR (VACUOLAR PROTON ATPASE-A3-large stokes shift *monomeric* Orange) reporter genes (Rips *et al.*, 2014; Nagashima *et al.*, 2020a) were introduced into the GFP–KOR1 CFP–SYP61 line and 15A2 by *Agrobacterium*-mediated transformation.

Arabidopsis ethyl methanesulfonate mutagenesis and mutant screening

Ethyl methanesulfonate (EMS)-mutagenized M_2 seeds were generated according to Kim *et al.* (2006). A total of 25 000 seeds (0.5 g) of GFP–KOR1 CFP–SYP61 were treated with 0.4% EMS for 8 h. The M_1 seeds were sown on 24 trays (~1000 seeds per tray). One tray was divided into eight compartments to create M_2 seed pools of 125 M_1 plants in each compartment. The inhibition assay of *N*-glycan maturation was performed using 2000 seeds from each pool. Mature M_2 seeds were harvested and sown on plates containing 1× Murashige and Skoog (MS) salts (Murashige and Skoog, 1962), 3% sucrose, 1.5% agar, 4 μM KIF (Carbosynth LLC), and stratified at 4 °C for 2 d. Plates were transferred to an incubator set at 25 °C and long-day conditions (16 h light/8 h dark) with 50% output of Phillips F17T8TL741 light bulbs for 4 d.

Mutant mapping

F_2 plants, following a cross between a mutant (in the Col-0 background) and Ler, were sown on 1× MS medium supplemented with 4 μM KIF to identify the genome mutation. These plants were analyzed using INDEL (insertion/deletion) markers for rough mapping. Fine mapping was carried out with bulk DNA of ~100 F_2 plants selected by KIF sensitivity and PCR analyses. For next-generation sequencing (NGS), the genomic DNA of 100 segregating F_2 mutant pools was extracted using the CTAB (cetyltrimethylammonium bromide) method. The sequencing library preparation and the Illumina-NGS run were performed at the Texas A&M Institute of Genome Sciences & Society core facility with a read length of 150 bp paired-ends. Sequencing reads were mapped to the Arabidopsis TAIR10 genome using Bowtie2 (version 2.2.4), allowing up to two mismatches. The mapping interval and candidate mutations were identified using the Galaxy platform.

Stress assays

To measure root growth, seeds were sown on plates containing 1× MS salts pH 5.8, 3% sucrose, and 1.5% agar before stratification at 4 °C for 2–4 d. Plates were moved to an incubator set at 25 °C and 16 h light/8 h dark long-day conditions using 50% output of Phillips F17T8TL741 light bulbs. Root positions were marked on the second day of culture for the KIF sensitivity test, and root growth was scored after an additional 4 d. For the salt stress assay, plants were germinated and cultured on a cellophane membrane on MS control medium as described previously (Koiwa *et al.*, 2003). After 4–5 d, plants on the cellophane membrane were moved to MS medium supplemented with 140 mM NaCl, and root tip positions were marked. Plants were incubated for 7 d before measuring final root lengths.

Protoplast preparation and transfection with plant expression constructs

The *ARFA1E* coding sequence was obtained by PCR from genomic DNA isolated from either the wild type (WT; Col-0) or 15A2 using primers ARFA1E_fw-XbaI and ARFA1E_rev-NcoI (see Supplementary Table S1) and cloned via *Xba*I/*Nco*I sites into plant expression vectors pGFP2-NX and pOFP2-NX behind the strong constitutive cauliflower mosaic virus (CaMV) 35S promoter. Vector modifications are described in Linnenbrügger *et al.* (2022).

To obtain protoplasts from Arabidopsis roots (Ryu *et al.*, 2019), seeds were surface-sterilized with ethanol (vortexing for 15 s each in 70% ethanol, absolute ethanol, and again 70% ethanol). Dried seeds were placed on plates containing 0.5× MS salts pH 5.8, 1% sucrose, and 1% agar (no cellophane or mesh), stratified at 4 °C for 2 d, and grown vertically under long-day conditions (16 h light, 22°C/8 h dark, 20 °C) in a plant growth chamber (Percival AR-41L3 with white LEDs adjusted to 130 μmol m^{-2} s^{-1}). At 5–7 d after sowing, the lower 1 cm of ~1000 seedlings were cut and placed in a 35 mm diameter sterile Petri dish containing 4 ml of enzyme solution (Ryu *et al.*, 2019) using 1.25% Cellulase 'Onozuka R-10®' (Serva) and 0.1% Macerozyme R-10® (Serva). After 2

h of incubation at room temperature, the solution was strained through a sterile 60 μm mesh. Centrifugation was carried out in a swing-out rotor (60 *g*) at room temperature, before protoplasts were transfected by the polyethylene glycol (PEG) method as described in Damm *et al.* (1989), starting by resuspension in artificial seawater (W5), but scaled down to 50 000–100 000 cells per sample, using only 5 μg of plasmid DNA, and reducing the time in PEG solution to 5 min. After 24 h dark incubation at room temperature, protoplasts were observed with a confocal laser-scanning microscope SP5 (Leica, Germany). All micrographs in this research are single-slice images. Image processing was conducted with the Leica application suite for advanced fluorescence (LAS AF).

Confocal microscopy

Stably transformed seedlings were observed with a Nikon FN-1 C1si confocal laser-scanning microscope and processed by NIS-Elements C (Nikon Instruments, USA). Five-day-old seedlings were used for the observations. For endocytosis analyses, the seedlings were soaked in 1× MS liquid medium supplemented with 25 μM FM4-64 for 5 min. The excess dye was washed off with 1× MS, and micrographs were taken at each time point. To investigate endocytic recycling, seedlings were incubated similarly in a liquid medium containing 50 μM brefeldin A (BFA) for 60 min, washed with 1× MS, and incubated for 60 min. The neighbor distance was measured by 2D particle distribution in an ImageJ plugin BioVoxxel Toolbox (10.5281/zenodo.5986130). The signal was measured from a total of 30 cells (five cells/plant×six plants). The details of each measurement are described in Supplementary Fig. S1.

Protein production

Recombinant proteins were expressed with N-terminal His (6×) tags and purified by Ni–NTA metal–chelate chromatography. Expression constructs pET30a-ARFA1C-WT, pET30a-ARFA1C-T31N, and pET30a-SEC7/BIG5 (587–791) were provided by Drs Manoj K. Singh and Gerd Jürgens (Singh *et al.*, 2018). The nucleotide sequence of ARFA1E was amplified by PCR from a cDNA clone (ABRC stock #G12397) using specific primers ARFA1E_F and ARFA1E_R, given in Supplementary Table S1, and cloned via *Nco*I/*Xho*I sites into vector pET30a, thereby replacing the BFA-inhibited guanine nucleotide exchange factor 5 (BIG5) coding sequence. The G69R mutation was introduced into the ARFA1E coding sequence by the quick-change mutagenesis method (Xia *et al.*, 2015) using primers 2111 arfa1e_R and 2112 arfa1e_F (Supplementary Table S1), and also cloned into the pET30a vector via *Nco*I/*Xho*I sites. Recombinant proteins were produced in *Escherichia coli* BL21 (DE3). Cells harboring the expression construct were induced with 0.4 mM isopropyl-β-D-1-thiogalactopyranoside and grown for 18 h at 16 °C. Cells were harvested by centrifugation and lysed by ultrasonication in lysis buffer (50 mM Tris–HCl pH 7.5, 200 mM NaCl, and 5% glycerol). The supernatant containing recombinant proteins was allowed to bind to the Ni–NTA resin (Bio-Rad Laboratories, USA), followed by washing with wash buffer (50 mM Tris–HCl pH 7.5, 200 mM NaCl, 20 mM imidazole). Bound proteins were eluted with elution buffer (50 mM Tris–HCl pH 7.5, 200 mM NaCl, 50 mM imidazole) and simultaneously concentrated-exchanged for GDP binding buffer (see below) using MilliporeSigma™ Amicon™ Ultra-4 Centrifugal Filter Units. The purity of the recombinant proteins was analyzed using 15% SDS–PAGE and quantified using Bio-Rad Protein Assay (Bio-Rad Laboratories, USA).

In vitro nucleotide exchange assay

The *in vitro* nucleotide exchange assay was conducted as described previously (Singh *et al.*, 2018) with some modifications. The GDP binding reaction was performed by incubating 50 μM of the ARF protein in 100 μl of GDP-binding buffer (20 mM HEPES-NaOH pH 7.5, 50 mM NaCl, 0.5 mM $MgCl_2$, 5 mM EDTA, 1 mM DTT). The reaction was initiated by adding 1.25 mM GDP (Thermo Fisher Scientific, USA) and incubated at 20 °C for 90 min. The reaction was stopped by adding $MgCl_2$ to a final concentration of 10 mM and subsequently incubated at 20 °C for 30 min. After exchange for nucleotide exchange buffer (40 mM HEPES-NaOH pH 7.5, 50 mM NaCl, 10 mM $MgCl_2$, 1 mM DTT), the GDP–GTP exchange reaction was performed with 1 μM ARF and 50 nM (purified recombinant) BIG5 protein in a volume of 100 μl. The reaction was initiated by adding 20 μM GTPγS (Millipore/Sigma, USA) at 37 °C. Tryptophan fluorescence was measured in a SpectraMax iD3 Multi-Mode Microplate Reader (Molecular Devices, LLC, USA) at excitation and emission wavelengths of 298 nm and 340 nm, respectively, for 20 min with a regular interval of 8 s. All reactions were performed in three technical replicates. Experiments were repeated twice with similar results.

Immunoblotting

Immunodetection of proteins with complex *N*-glycans was conducted essentially as described previously (Jeong *et al.*, 2018) using rabbit anti-horseradish peroxidase (Sigma P7899) as the primary antibody (α-HRP) and goat anti-rabbit IgG–HRP conjugate as the secondart antibody.

Reverse transcription–PCR

To investigate *ARFA1E* mRNA accumulation in *arfa1e-2*, total RNA was extracted from 10-day-old seedlings with Trizol (Thermo Fisher Scientific, USA) according to the manufacturer's protocol. Reverse transcription using 500 ng of total RNA was performed using GoScript™ (Promega, USA) according to the manufacturer's protocol. PCR was conducted using 1/20th of the reverse transcription reaction and primers N434 arfa1e-2RT_F and N397 arfa1e-2R for *ARFA1E*, with actin primers E161 AtACT2_F and E162 AtACT2_R as positive control (see Supplementary Table S1).

ARFA1E complementation

Plant transformation constructs for complementation were prepared by PCR amplification of *ARFA1E* genomic fragments using the bacterial artificial chromosome (BAC) plasmid T17J13 as a template. For the WT, the full-length fragment, including the 1.5 kbp promoter region, the 2.2 kbp coding region, and the 0.5 kbp terminator region, was amplified using primer pair 2271 ARFA1EgF and 2272 ARFA1EgR (Supplementary Table S1). For $ARFA1E^{G69R}$, two fragments were prepared by PCR using primer pair 2271 and 2111 arfa1eR, or primer pair 2273 ARFA1EmF and 2272 (Supplementary Table S1). The WT fragment and the combined mutant fragments were cloned into *Sma*I-digested pEntr2B plasmid (Thermofisher, USA) using the ClonExpress Ultra One Step Cloning Kit V2 (VAzyme, PRC). The entire sequence was verified by whole plasmid sequencing (Eurofins, USA). Subsequently, the *ARFA1E* variants were inserted into pMDCGAT-GW (modified from pMDCGAT; Vikram and Koiwa, 2009) using the Gateway LR reaction, and resulting pMDC-ARFA1E binary vectors were introduced into *Agrobacterium tumefaciens* GV3101. Mutant *arfa1e-2* plants containing GFP–KOR1 or BiP–*m*Cherry (Rips *et al.*, 2014) were transformed by the flower-dip method with agrobacteria harboring the WT or mutant pMDC-ARFA1E version. ARFA1E transformants were selected on media containing 0.4 mM glyphosate.

Accession numbers

15A2/ARFA1E (AT3G62290); ARFA1C/BEX1 (At2g47170); CGL1/GNT1 (AT4G38240); COBRA (AT5G60920); FLA4/SOS5 (AT3G46550); PHT4;6 (AT5G44370); PRC/CESA6/IRX2 (AT5G64740); RSW2/KOR1 (AT5G49720); STT3A (AT5G19690).

Results

Isolation of mutants with high sensitivity to kifunensine, an α-mannosidase I-specific inhibitor

Little is known about the physiological targets of the plant *N*-glycan modification pathway, which is partially due to the lack of a suitable genetic system to identify gene products that interact with *N*-glycan modifications. We previously reported that genetic interaction between the *KOR1* mutant line *rsw2-1* and complex *N*-glycan biosynthesis mutations causes severe root growth defects in plants (Kang *et al.*, 2008), suggesting that root growth can be used as a phenotypic output for complex *N*-glycan dependency.

To conditionally induce complex *N*-glycan deficiency in Arabidopsis plants, we used KIF, a specific inhibitor of α-mannosidase I enzymes (Elbein *et al.*, 1991). Basal media conditions were set to 1× MS, 3% sucrose, previously optimized for salt stress screening for Arabidopsis (Wu *et al.*, 1996; Zhu *et al.*, 2002; Koiwa *et al.*, 2003; Kang *et al.*, 2008) and was expected to impose mild osmotic stress. Decreasing the media strength required a higher concentration of KIF and, therefore, was avoided. Inhibition of multiple ER and Golgi a-mannosidase I isoforms may interfere not only with complex *N*-glycan formation but also with ER protein quality control, triggering growth inhibition by KIF itself. Therefore, we first determined the KIF sensitivity of WT and mutant Arabidopsis lines so that KIF could be used as a genetic screening tool. As wild-typical references, we used Col-0 and the parental GFP–KOR1 CFP–SYP61 reporter line [*rsw2-1* complemented by a genomic GFP–KOR1 construct and an introgressed TGN marker CFP–SYP61 (Rips *et al.*, 2014)], and as mutant references untransformed *rsw2-1* (Liebminger *et al.*, 2009) and GFP–KOR1 introgressed into the *pht4;6* mutant background with a compromised phosphate transporter in the Golgi apparatus (Hassler *et al.*, 2012). In germination and growth assays, 4 μM KIF strongly inhibited root growth of GFP–KOR1 *pht4;6*, but plants were viable after being rescued (Fig. 1A). Under the same condition, *rsw2-1* showed much more severe growth inhibition, with plants not being viable after rescue. Higher KIF concentrations also inhibited the growth of Col-0 and the GFP–KOR1 CFP–SYP61 line, perhaps due to the inhibition of multiple ER and Golgi a-mannosidase I involved in complex *N*-glycan formation and ER protein quality control. When *N*-glycan profiles were visualized by immunoblotting with anti-HRP antibodies, total extracts of Col-0 WT plants showed substantially reduced complex *N*-glycan patterns upon germination on 4 μM KIF (Fig. 1B), whereas the *cgl1-3* control (T-DNA allele; Frank *et al.*, 2008) showed a total lack of complex *N*-glycan signals.

Forward genetic screening was conducted using 380 000 M_2 plants of the EMS-mutagenized GFP–KOR1 CFP–SYP61 line. The GFP–KOR1 CFP–SYP61 line was used for secondary selection to find KIF-sensitive mutants with altered KOR1 dynamics in the cell. Seeds were germinated on 1× MS agar medium containing 4 μM KIF and placed vertically (Fig. 1C). Plants developing short swollen roots were rescued, and their M_3 progenies were tested for root growth under conditions with or without KIF. Based on the root phenotypes, we classified the obtained mutants into three groups: class-I plants with normal root growth on MS media and KIF hypersensitivity; class-II plants with shorter roots than GFP–KOR1 CFP–SYP61 on MS and KIF hypersensitivity; and class-III plants with swollen root tips on MS with or without KIF (Fig. 1D). In this study, we chose to focus on candidates from the isolated 50 class-I and 58 class-II mutant lines, respectively.

KIF sensitivity of class-I and class-II mutant plants was determined using a root growth assay. The sensitivity index (root length with KIF/root length without KIF) was calculated for each mutant line and is shown in Supplementary Fig. S2. This index revealed a wide range of KIF susceptibility (~95% to 30% inhibition) among the isolated mutant lines. Similarly, the salt sensitivity index was determined for each mutant because complex *N*-glycan- and cell wall-related mutations often result in salt sensitivity (Kang *et al.*, 2008; Liebminger *et al.*, 2009; Colin *et al.*, 2023; Supplementary Fig. S3). Although many mutants exhibited salt hypersensitivity, several did not (Supplementary Fig. S3A, B). Analysis of the KIF and salt sensitivity indexes showed no significant correlation (Supplementary Fig. S3C), suggesting that multiple mechanisms can lead to KIF sensitivity.

To identify the underlying mutations in representative KIF-sensitive lines, we conducted NGS-based mapping of the selected defects. Upon identification of candidate base changes, each mutant was tested by crossing with a corresponding T-DNA insertion line. This analysis showed that five lines are allelic to mutants previously shown to be KIF sensitive (Fig. 2). Gene mutations were found in class-I mutant 8D4 that was allelic to the glycosylphosphatidylinositol (GPI)-anchored glycoprotein gene *COBRA* (Roudier *et al.*, 2005), and in 5A4 and 10C5 that were allelic to *PROCUSTE1* (Fagard *et al.*, 2000), equivalent to the cellulose synthase complex subunit gene *CESA6/IRX2*. Similarly, 22A5 and 9D10 were allelic to *FLA4/SOS5*, affecting a fasciclin-type arabinogalactan protein found in plant cell walls (Johnson *et al.*, 2003; Shi *et al.*, 2003), or *PHT4;6*, encoding a Golgi-located phosphate transporter, respectively. Identification of these mutations confirmed that our large-scale screening is in line with previous observations (Liebminger *et al.*, 2009; Hassler *et al.*, 2012), reinforcing the strong linkage between complex *N*-glycan formation in the Golgi apparatus and cell wall biogenesis at the plasma membrane.

Class-I mutant 15A2 showed abnormal TGN morphology due to an inactive version of ARFA1E

To identify novel links that connect KIF sensitivity to cellular glycoprotein dynamics, we investigated the subcellular localization of the GFP–KOR1 reporter in the mutant lines and found several with abnormal GFP–KOR1 localization patterns,

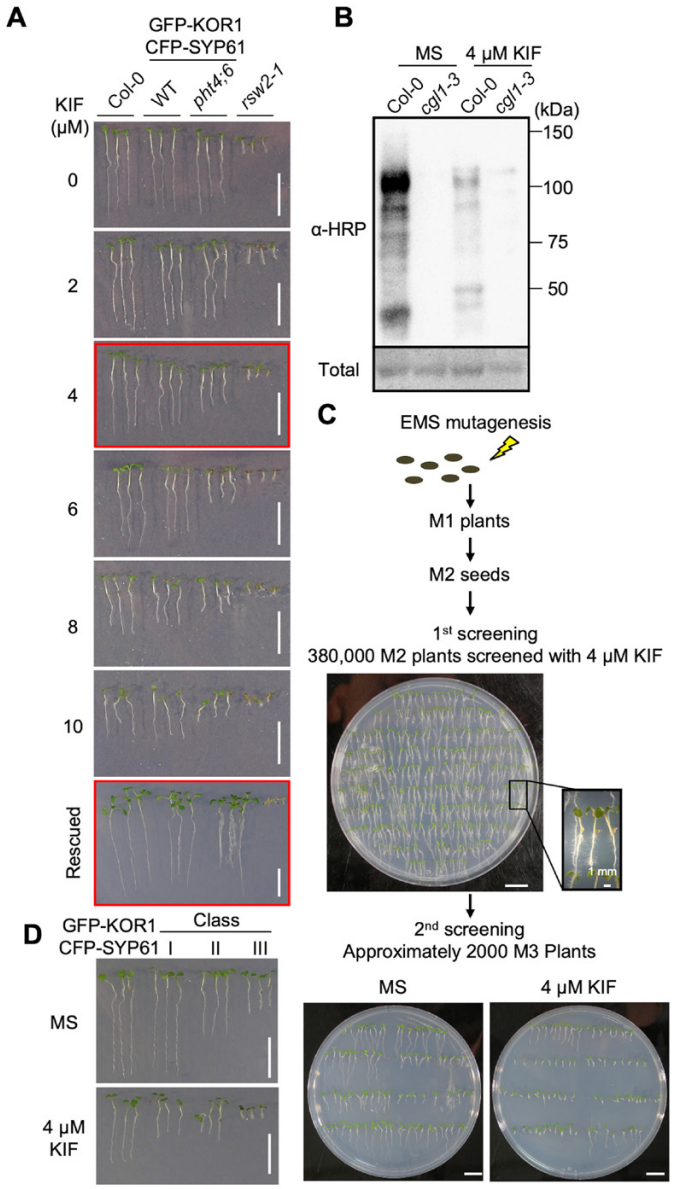

Fig. 1. Screening for KIF-hypersensitive mutants. (A) Plant growth responses to different kifunensine (KIF) concentrations. Plants were grown on 1× MS medium or supplemented with the indicated KIF concentrations for 5 d, and photographed. To investigate recovery from KIF stress, plants grown on 1× MS with 4 μM KIF were transferred to MS medium without KIF and cultured for an additional 5 d (red frames) to monitor recovery from potential damage (Rescued). (B) Immunodetection of complex-type *N*-glycans using anti-horseradish peroxidase antibodies (α-HRP). A 4 μg aliquot of protein extract was separated by SDS–PAGE in each lane. Ponceau-S staining of the blot membrane is shown as loading control below (Total). (C) Screening procedure of this study. The GFP–KOR1 CFP–SYP61 line was used for EMS mutagenesis (for details, see the Materials and methods). A frame on the plate shows the position of magnified seedlings on the right. (D) Representative plants from each phenotype class. Plants were grown on 1× MS medium or supplemented with 4 μM KIF for 5 d. The scale bars represent 10 mm unless indicated otherwise.

similar to our previous report (Nagashima *et al.*, 2020b). In this study, we focused on class-I mutant 15A2 with aggregated TGN structures (Fig. 3A). 15A2 was crossed with its parental line twice and then allowed to self-pollinate ($15A2_{BC2}$). Since the back-crossed plants again showed TGN aggregation and KIF-hypersensitive root growth (Fig. 3A, B), $15A2_{BC2}$ was used for further phenotypic characterization and is referred to as 15A2 hereafter.

Map-based cloning and genome sequencing analysis identified a Gly-to-Arg substitution at the 69th amino acid of ARFA1E (At3g62290) (Fig. 4A; Supplementary Fig. S4A, B). ARFA1E is a member of the ARF protein family of small GTPases, which has been shown to localize to the Golgi apparatus and TGN of the secretory system (Gebbie *et al.*, 2005; Robinson *et al.*, 2011). Its activity is controlled by binding GTP or GDP. The GDP-bound, inactive ARF protein resides in the cytoplasm, whereas the GTP-bound active ARF form attaches to vesicles. Surprisingly, a T-DNA insertion allele of ARFA1E (*arfa1e-2*), which does not express *ARFA1E* (Supplementary Fig. S4A, C; see below for further explanation), did not produce abnormal TGN shapes (as judged by GFP–KOR1) and also did not show KIF-sensitive root growth (Fig. 3A, B). Interestingly, the 15A2 mutation occurred in a region overlapping with the GTP-binding domain and switch domain II (Supplementary Fig. S4B). GDP–GTP exchange in ARF is catalyzed by the SEC7 domain of ARF-GEFs, such as in BIG5 (Singh *et al.*, 2018). When complex *N*-glycan levels in 15A2 were analyzed by anti-complex *N*-glycan immunoblot (anti-HRP), 15A2 did not show significant difference from the parental line in either the absence or presence of 4 μM KIF, indicating that $ARFA1E^{G69R}$ does not affect the biogenesis of the complex *N*-glycan itself (Supplementary Fig. S4D).

To determine the effect of the G69R mutation on ARFA1E function, we tested the GDP–GTP exchange activity of the recombinant WT protein (ARFA1E-WT) and the G69R version without or in combination with the SEC7 domain of BIG5 (Fig. 4B–D). In addition, ARFA1C-WT and ARFA1C with the T31N mutation ($ARFA1C^{T31N}$), a known defect in GDP–GTP exchange that keeps the protein in an inactive state, were used as controls. In this assay, GDP–GTP exchange activity was detected as a steady increase in the fluorescence intensity of the reaction mixture. The fluorescence intensity of ARFA1C, but not $ARFA1C^{T31N}$, increased in the presence of BIG5 and GTPγS (Fig. 4C). Similarly, ARFA1E showed an increase in fluorescence intensity, yet no increase was detected for $ARFA1E^{G69R}$ (Fig. 4D). These results suggest that the G69R change impairs BIG5-mediated GDP–GTP exchange on ARFA1E, keeping the protein in the GDP-bound inactive form.

The $ARFA1E^{G69R}$ exchange affects the morphology of multiple secretory organelles

To investigate the effect of the G69R mutation on the subcellular localization of ARFA1E, we transiently expressed ARFA1E–reporter fusions in Arabidopsis root protoplasts. When expressed in Col-0 cells, the ARFA1E-WT version was observed in intracellular particles and the cytoplasm (Fig.

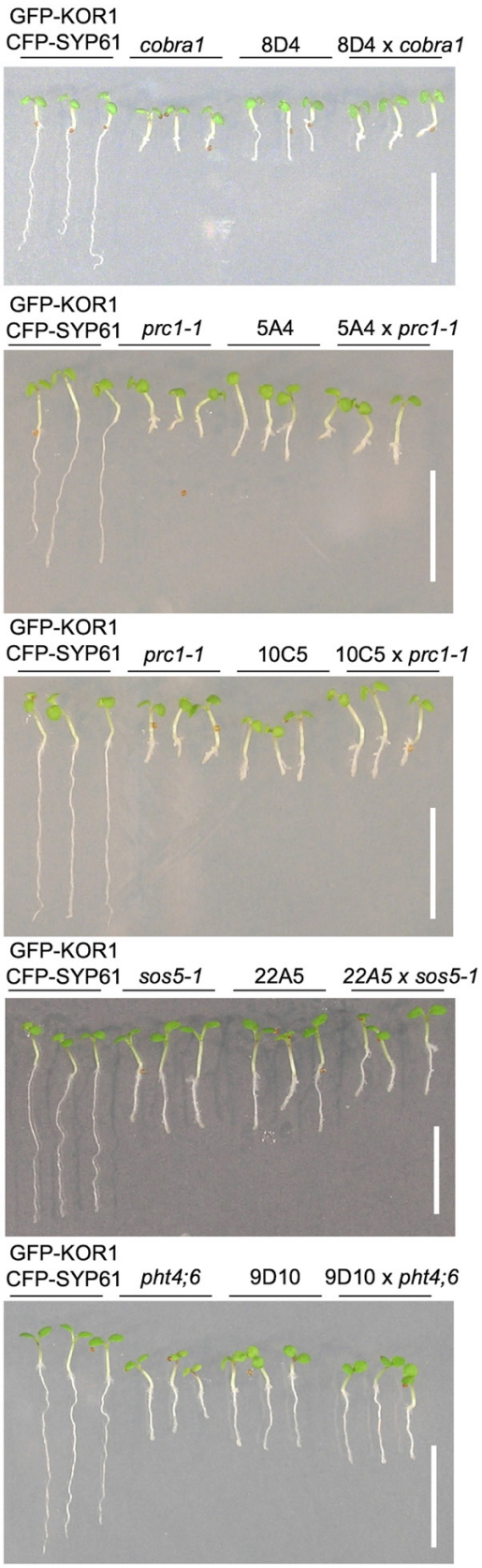

Fig. 2. Identification of causal genes in different KIF-hypersensitive mutants by allelism tests. GFP–KOR1 CFP–SYP61, previously characterized lines of the candidate mutants, and F_1 plants of the indicated crosses (further explained in the text) were grown on 1× MS medium with 4 μM KIF for 5 d. The scale bars represent 10 mm.

5A, top), whereas the G69R variant predominantly localized in the cytoplasm, consistent with the pattern found for dysfunctional GDP-locked forms of ARFA1 (Xu and Scheres, 2005). The precise localization of ARFA1E was tested by co-expression with three different markers, namely GNTI for the *cis*-Golgi, MANII for the *medial*-Golgi, and SYP61 for the TGN. ARFA1E showed the highest overlap with the *cis*-Golgi marker but also co-localized with the other two Golgi markers (Fig. 5B). We therefore concluded that ARFA1E broadly distributes over the Golgi apparatus and TGN as previously reported for ARFA1C (Robinson *et al.*, 2011). Interestingly, in 15A2 cells with endogenous ARFA1E^{G69R}, both the G69R and WT versions of ARFA1E showed a cytoplasmic accumulation profile (Fig. 5A, bottom), indicating that endogenous ARFA1E^{G69R} interferes with proper localization of other ARFA1 isoforms, which is integral to their function.

When expressing the orange fluorescent protein (OFP) ER marker in root protoplasts, we noticed that ARFA1E^{G69R} changes the morphology of the ER (Fig. 5A), which was especially obvious in the 15A2 background. To investigate ARFA1E^{G69R} in whole plants, we introduced another ER marker, BiP–*m*Cherry, into GFP–KOR1 CFP–SYP61, 15A2, and *arfa1e-2*. In parental GFP–KOR1 CFP–SYP61, the ER showed a reticular pattern in root tip cells, whereas torpedo-shaped ER bodies were additionally observed in hypocotyl and cotyledon cells (Fig. 5C; Supplementary Fig. S5, white arrowheads). In the 15A2 background, aggregated spherical ER patterns prevailed (Fig. 5C center; Supplementary Fig. S5, top). This supports the idea that ARFA1E is needed to maintain normal ER morphology. Of note, the *arfa1e-2* T-DNA insertion mutant showed ER patterns indistinguishable from the original GFP–KOR1 CFP–SYP61 line (Fig. 5C, right).

Overexpression of *ARFA1E^{G69R}* induced abnormal ER shapes in protoplasts (i.e. spherical aggregations of various sizes) even though the functional allele of ARFA1E was present in Col-0 host cells (Fig. 5A). This was also seen in 15A2 cells, which express *ARFA1E^{G69R}* from the native genomic context (Fig. 5A, B; Supplementary Fig. S5, middle). To confirm that a dominant-negative effect of endogenous ARFA1E^{G69R} is the cause of abnormal organelle morphologies observed in 15A2, we crossed 15A2 containing BiP–*m*Cherry with Col-0 WT and the T-DNA insertion line *arfa1e-2* (Supplementary Fig. S5, bottom). The organellar phenotype was observed in F_1 plants based on GFP–KOR1 and BiP–*m*Cherry. Upon both crosses, the ER morphology in hypocotyls of the F_1 plants lacked characteristic oval-shaped ER bodies in all combinations. F_1 plants from the 15A2×*arfa1e-2* cross showed spherical aggregations like parental 15A2, which were less evident in the F_1 of 15A2×Col-0, indicating that the G69R effect was incomplete in the presence of a WT allele. To establish that

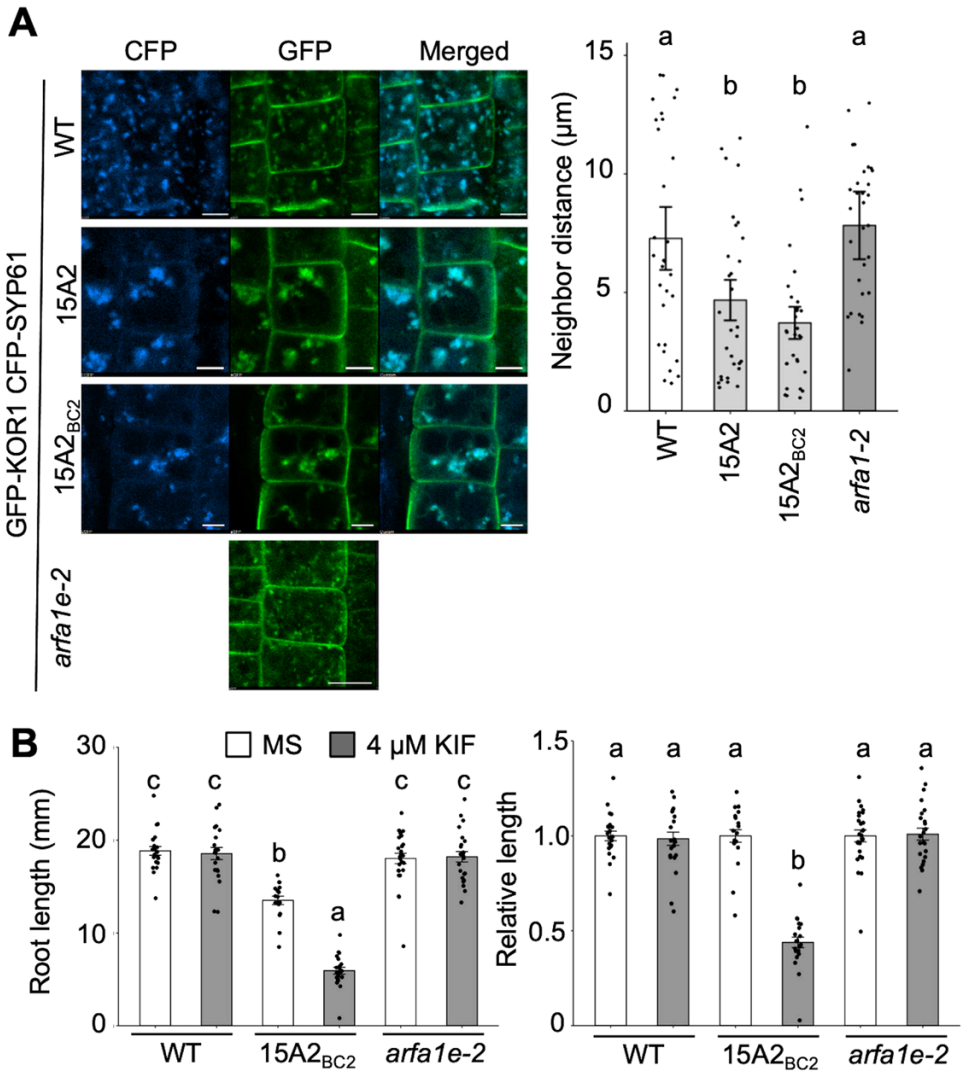

Fig. 3. KIF-sensitive mutant line 15A2 showed abnormal TGN morphology. (A) Microscopic images with quantification of neighbor distance between GFP–KOR1 particles in parental GFP–KOR1 CFP–SYP61 (WT), 15A2, 15A2$_{BC2}$ (back-crossed twice), and T-DNA line *arfa1e-2*. CFP panels show the TGN marker SYP61–CFP. Note that GFP–KOR1 in *arfa1e-2* is an independent transformation event. Four-day-old seedlings were used for the observation. Scale bars represent 10 μm. The neighbor distance was determined with BioVoxxel 2D Particle Distribution in ImageJ. Error bars represent the SEM, *n*=30. (B) Raw (left) and relative (right) root growth of GFP–KOR1 CFP–SYP61, 15A2$_{BC2}$, and *arfa1e-2* on 1× MS medium without (white bars) or with (gray bars) 4 μM KIF. Root growth was plotted after 5 d. Error bars represent the SEM, *n*=17–25. Different letters indicate significant differences ($P<0.05$) between genotypes (one-way ANOVA followed by Tukey's honestly significant difference post-hoc test).

the *ARFA1E*^{G69R} allele is the cause of organellar morphology alterations, *arfa1e-2* lacking functional *ARFA1E* was complemented with an *ARFA1E* genomic fragment with or without the base change causing the G69R mutation. *GFP-KOR1* and *BiP*-m*Cherry* markers were co-transformed with the *ARFA1E* constructs. In fact, transformation of *arfa1e-2* with *ARFA1E*^{G69R}, but not the WT *ARFA1E* genomic fragment, reproduced TGN aggregation (visualized by GFP–KOR1), as well as altered ER morphology, with a lack of ER bodies (visualized by BiP–*m*Cherry, Supplementary Fig. S6). These results unequivocally established that *ARFA1E*^{G69R} is causal for the 15A2 phenotype.

The morphologies of Golgi stacks and the TGN were assessed using xylosyltransferase (XYLT)–*m*Cherry introgressed into GFP–KOR1 CFP–SYP61 and 15A2 (Fig. 5D). In the parental line, GFP–KOR1 and XYLT–*m*Cherry accumulated in particle-shaped, adjacent dots [merger of the red fluorescent protein (RFP) and GFP channels]. In 15A2, XYLT–*m*Cherry labeled aggregated structures that substantially overlapped with the GFP–KOR1 signals, indicating that the Golgi apparatus did not form properly, with less distinction between Golgi stacks and the TGN. On the other hand, in contrast to the cells overexpressing ARFA1C^{T31N} (Lee *et al.*, 2002), the aggregated Golgi apparatus and TGN did not overlap with the ER in the

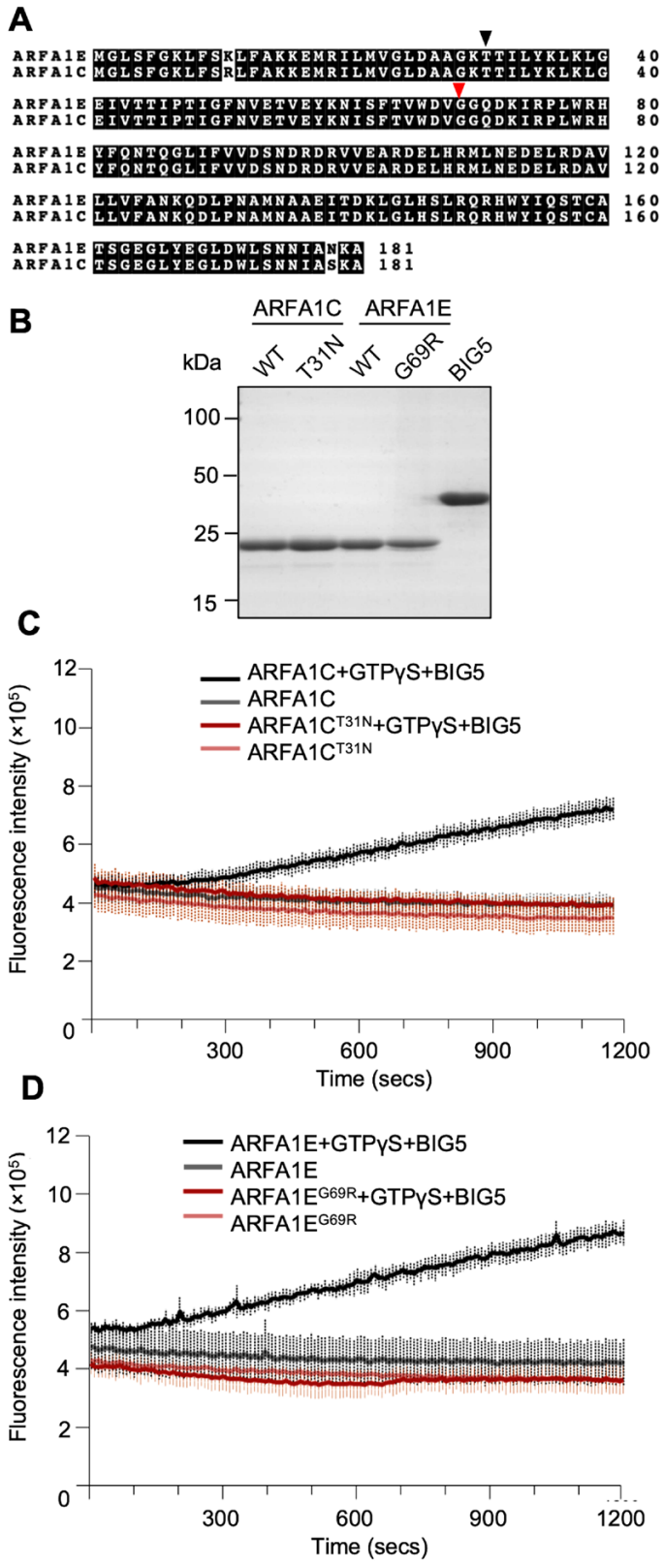

Fig. 4. The G69R mutation impairs GDP–GTP exchange on ARFA1E. (A) Amino acid sequence alignment of ARFA1E and ARFA1C. The black and red arrowheads point to threonine T31 and glycine G69, respectively. (B) Coomassie brilliant blue-stained gel upon SDS–PAGE of purified 6×His-tagged ARFA1C wild type (WT), ARFA1C^{T31N}, ARFA1E-WT, ARFA1E^{G69R}, and BIG5. (C, D) *In vitro* GDP–GTP exchange activity of BIG5 on ARFA1C (WT) versus ARFA1C^{T31N} (C), and ARFA1E (WT) versus ARFA1E^{G69R} (D). The plotted increases in tryptophan fluorescence correspond to a conformational change—from the GDP-bound to the GTPγS-bound state. Error bars represent the SD, n=3.

15A2 cells (Supplementary Fig. S7), suggesting that fusion between the ER and Golgi/TGN did not occur in 15A2.

Tonoplast morphology was visualized using VHA-A3-Lss*m*OR. In the parental line GFP–KOR1 CFP–SYP61, VHA-A3-Lss*m*OR labeled the tonoplast membrane as well as the TGN (Supplementary Fig. S8, top, white signals in the merged channels). In 15A2, the *m*OR signal labeled more aggregated TGN/early endosomes (EEs), but tonoplast membranes appeared largely unaffected. Similarly, cell plate formation was normal in 15A2 (Supplementary Fig. S8, bottom). Overall, ARFA1E^{G69R} seems to selectively impact the morphology of the ER and the Golgi apparatus.

The ARFA1E^{G69R} exchange has broad impacts on the secretory pathway

To assess the impact of ARFA1E^{G69R} on the dynamic nature of vesicular transport, we analyzed endocytosis and endocytic recycling. To test endocytic recycling, plants were treated with BFA, and GFP–KOR1 transport was monitored within the cells. Incubation with BFA produced BFA bodies in both the parental GFP–KOR1 CFP–SYP61 line and 15A2 (Fig. 6A). When BFA was washed out, BFA body formation was abolished in cells of the parental GFP–KOR1 CFP–SYP61 line, but not in 15A2, which coincided with a later appearance of GFP signals at the plasma membrane. This observation suggested that endocytic recycling in 15A2 is much slower than in the WT. Next, endocytic activity was tested by internalization of the amphiphilic dye FM4-64. During a time course of 180 min incubation after FM4-64 treatment, the plasma membrane-to-intracellular signal ratios remained significantly higher in 15A2 compared with GFP–KOR1 CFP–SYP61 (Fig. 6B). No significant difference of FM4-64 was observed between GFP–KOR1 CFP–SYP61 and 15A2 at 5 min after treatment. Still, the significant differences were detected after 30 min. This indicates that 15A2 has a delay in post-endocytic trafficking.

Slowing down vesicular transport processes increases stress sensitivity

Endocytic recycling and endocytosis are integral parts of stress acclimation in eukaryotes, from unicellular yeast (Lemière *et al.*, 2021) to mammals, including plants (reviewed in López-Hernández *et al.*, 2020), requiring dynamic reconfiguration of the cell wall and apoplastic components via the plasma membrane (reviewed in Fan *et al.*, 2015; Paez-Valencia *et al.*,

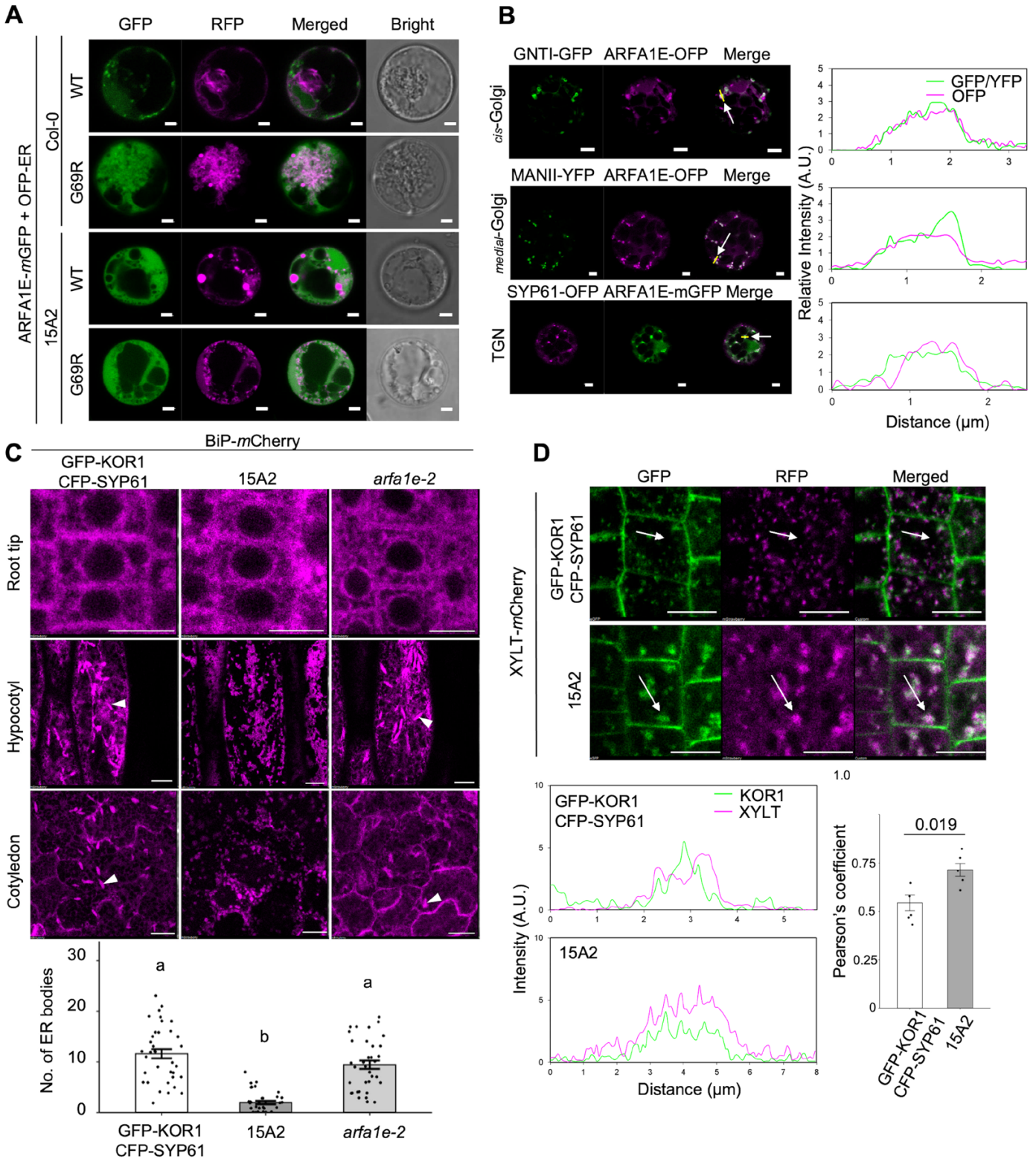

Fig. 5. The ARFA1E^{G69R} mutation impacts the morphology of the ER and the Golgi apparatus. (A) Transient co-expression of ARFA1E–*m*GFP (WT) or the mutant variant (G69R) with an ER marker OFP–ER in Arabidopsis root protoplasts. White signals in the merged GFP/RFP channels show partial co-localization of G69R with an abnormally shaped ER. Scale bars represent 3 μm. (B) Co-localization of ARFA1E with *cis*-, *medial*-, and *trans*-Golgi markers in Arabidopsis root protoplasts. The relative GFP/YFP and RFP signal intensities along the yellow lines indicated by the white arrows are shown in the line graphs. (C) Micrographs of an ER marker BiP–*m*Cherry in different seedling tissues and the number of ER bodies in roots of GFP–KOR1 CFP–SYP61, 15A2 (with dominant-negative G69R change), and *arfa1e-2*. Three-day-old plants were used for the observations. White arrowheads point to ER

bodies. The scale bars represent 10 µm. Error bars are the SEM, *n*=36. Different letters indicate significant differences (*P*<0.05) between the genotypes (one-way ANOVA followed by Tukey's honestly significant difference post-hoc test). (D) Micrographs of a Golgi marker XYLT–*m*Cherry in GFP–KOR1 CFP–SYP61 and 15A2. The graphs below show the signal intensities of XYLT and KOR1 along the white arrows drawn across single accumulations. The bar graph on the right shows the calculated Pearson's coefficient between GFP–KOR1 and XYLT–*m*Cherry. The number in the graph indicates the significant result of the Student's *t*-test (*P*<0.05). Error bars are the SEM, *n*=5.

2016). As our initial survey indicated, 15A2/*ARFA1E*^{G69R} plants showed enhanced sensitivity to high concentrations of NaCl and also KCl. However, sensitivity to mannitol, a non-ionic osmolyte, did not change significantly (Fig. 7A, B). Thus, higher ionic stress seems causal for the observed root growth inhibition. To test whether ARFA1E^{G69R} impacts the vesicle transport of proteins needed for cellulose biosynthesis during salt stress (Nagashima *et al.*, 2020a), we inspected NaCl-induced internalization of KOR1 from the plasma membrane, which is an integral part of root stress tolerance. In the parental line, transient internalization of GFP–KOR1 started 4 h after salt treatment (Fig. 7C, top).

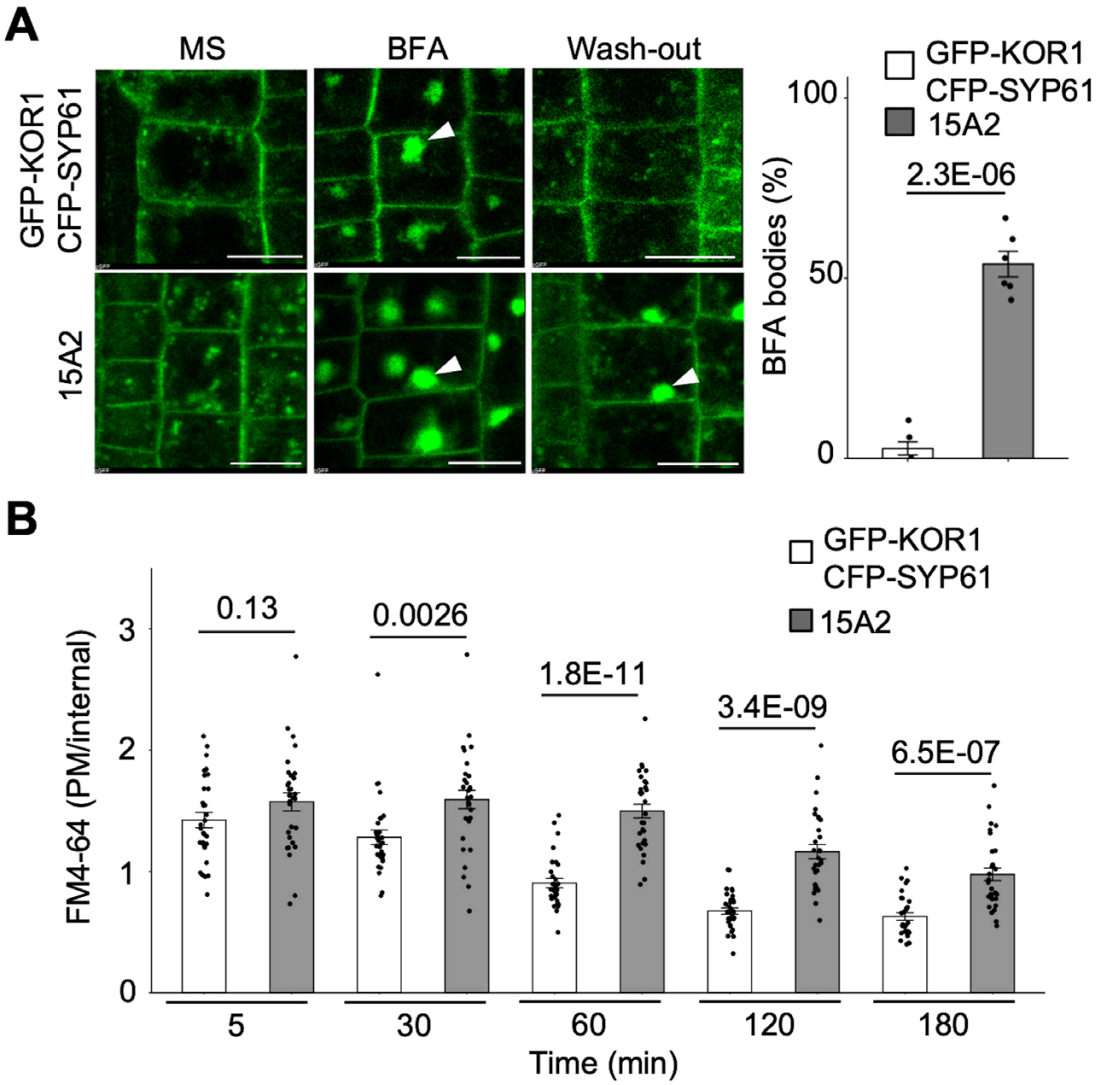

Fig. 6. The ARFA1E^{G69R} mutation affects endocytic recycling and endocytosis. (A) Assay pf recovery from BFA treatment to measure endocytic recycling activities. GFP–KOR1 CFP–SYP61 and 15A2 were incubated with 50 µM BFA for 60 min. BFA was washed out and the seedlings were incubated for an additional 60 min. The white arrowheads point to individual BFA bodies. Scale bars represent 10 µm. Right, the percentage of BFA bodies was calculated as the number of BFA bodies counted divided by the number of cells. Error bars represent the SEM, *n*=6. (B) Internalization efficiency of FM4-64 by endocytosis activities. The method for calculating the plasma membrane to internal FM4-64 ratio is given in Supplementary Fig. S1. Error bars represent the SEM, *n*=30. The numbers in both graphs indicate the result of the Student's *t*-test.

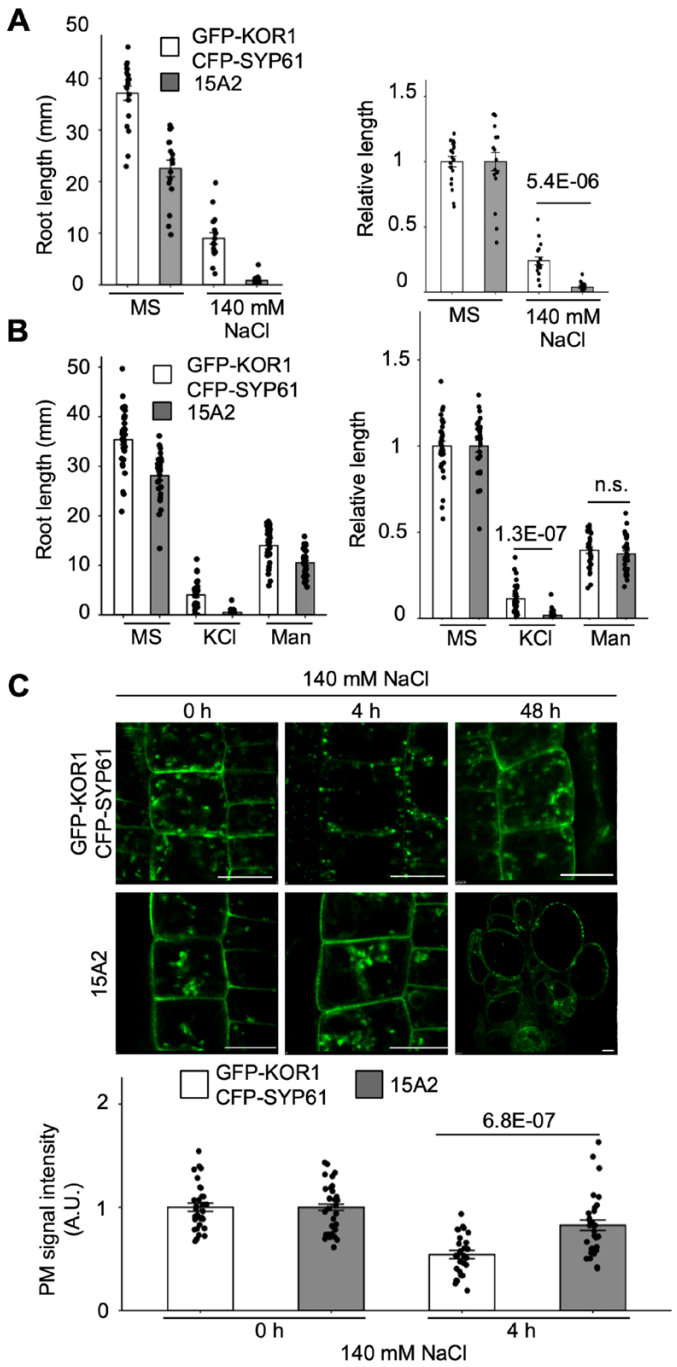

Fig. 7. 15A2/ARFA1E^{G69R} exhibits high sensitivity to salt stress. Root growth of GFP–KOR1 CFP–SYP61 and 15A2 on 1× MS medium with or without 140 mM NaCl (A), and 140 mM KCl or 300 mM mannitol (B). The left graphs show the actual root growth, and the right graphs the relative root growth (compared with the root length on 1× MS medium in each genotype). Error bars represent the SEM, *n*=14–33. (C) GFP–KOR1 CFP–SYP61 and 15A2 on 1× MS medium with or without 140 mM NaCl. Seedlings were germinated on a cellophane membrane placed on 1× MS medium and grown until day three prior to transfer to 1× MS medium with or without 140 mM NaCl. The bottom graph shows the relative GFP signal intensity at the plasma membrane (compared with 0 h in each genotype). Error bars represent the SEM, *n*=15. The numbers in the graphs show the result of the Student's *t*-test. n.s. stands for not significant; A.U. for arbitrary units.

In 15A2, a significantly higher amount of GFP–KOR1 was retained at the plasma membrane, especially obvious after 4 h of salt stress (Fig. 7C, bottom). After 48 h of salt treatment, 15A2/*ARFA1E*^{G69R} showed deformations similar to cells expressing endocytosis-defective KOR1 (Nagashima *et al.*, 2020a). This result strongly indicates that non-functional ARFA1 interferes with the stress-induced internalization of membrane (glyco)proteins, such as KOR1, thus contributing to salt sensitivity in Arabidopsis.

Discussion

To gain insight into the physiological role of *N*-glycosylated proteins in plants, we performed a forward genetic screen to obtain conditional mutants that reflect the requirement for operation of the *N*-glycan maturation pathway in the Golgi apparatus. After optimizing the concentration of the mannosidase-I inhibitor KIF, we obtained a suite of mutants whose root growth is affected when complex *N*-glycan production is blocked. The isolated mutant lines showed a wide range of impairment by KIF; however, salt sensitivity did not always correlate with KIF sensitivity, implying the existence of diverse targets that are affected by either impaired *N*-glycan maturation or complex *N*-glycan deficiency (like *cgl1*). Several mutations were mapped to a range of biosynthetic genes involved in cell wall formation, confirming the previously established connection between *N*-glycan maturation and cellulose biosynthesis. In addition, we identified a dominant-negative mutation in ARFA1E, which is a regulatory G-protein in eukaryotic vesicular transport (Yorimitsu *et al.*, 2014). The discovery of a new ARFA1E allele in this screening is an indication that there are functional interactions between the *N*-glycan maturation process in the luminal side of the endomembrane and soluble factors of the cytoplasmic, G-protein-based regulatory mechanism.

The 15A2 line contains the unique ARFA1E mutation that induced morphological changes in multiple organelles of the secretory system, namely the ER, Golgi stacks, and the TGN, albeit not affecting the vacuole or cell plate formation. This provides a unique genetically tractable system to analyze the function of ARFA1E. To date, no ARFA1 family T-DNA mutant lines with phenotype have been reported, and antisense lines that simultaneously target multiple ARFA1 genes produced growth retardation, but no cell-level phenotype has been associated even with the severe transgenic line (Gebbie *et al.*, 2005). ARFA1 antisense transgenic plants produced smaller cell size and smaller statue, together with slight changes in cell wall sugar composition; however, other constitutive traits have not been described. By contrast, the 15A2 line shed light on several important aspects of ARFA1E. First, we showed biochemically that 15A2 produces ARFA1E^{G69R}, a new GDP-locked form of ARFA1. Interestingly, the G69R mutation is located close to Q71, the mutation of which is known to cause

a constitutively active form of ARFA1 (Q71L). Yet G69R produced opposite results, namely the GDP-locked form. Because G69 is flanking the switch II region, which interfaces with GEF and changes conformation between the GTP- and GDP-bound form (Goldberg, 1998), replacing G69 with a bulky R residue could interfere with the proper conformation for GTP binding, thus preventing activation of mutant ARFA1E protein. Accumulation of ARFA1E^{G69R} in the cytoplasm is consistent with being the GDP-locked form. It is not known if the GDP-locked form of ARFA1 homologs is more or less stable than WT proteins; however, G69R stabilizes the GDP-bound form of ARFA1E, thus naturally increasing the dosage of the GDP-bound form in the cell. The data we provided for the subcellular organellar phenotype of ARFA1E^{G69R} have further significance. Previous studies on the dominant-negative form of ARFA1 family genes have used ectopic overexpression utilizing the 35S promoter (Lee *et al.*, 2002) or a heat shock-inducible promoter (Tanaka *et al.*, 2014). The overexpression approach results in a massive amount of the mutated dominant-negative form of ARFA1 protein, which probably causes extensive pleiotropic effects. By contrast, ARFA1E^{G69R} in the 15A2 and reverse-complemented lines is driven by the native promoter. The fact that endogenous ARFA1E^{G69R} produced a distinct subcellular organellar phenotype is an indication that ARFA1E is a biologically relevant member of the ARFA1 family.

The 15A2 line expressing ARFA1E^{G69R} in the native genomic context provided us with an opportunity to re-evaluate the ARFA1 family protein function previously suggested based on overexpression/gene silencing phenotype. In this context, it is important to note that the 15A2 host expressing the native promoter-driven ARFA1E^{G69R} can potentially induce mislocalization of WT ARFA1 proteins in the cell (Fig. 5A). Unlike the antisense ARFA1C line previously reported, the 15A2 line did not produce constitutive severe growth defects. The function of ARF1 in the maintenance of the ER morphology and formation of the Golgi and post-Golgi organelles has been proposed based on the overexpression phenotype of ARFA1C^{T31N} in protoplasts. Tobacco cells overexpressing ARFA1C^{T31N} produce a disorganized ER, fusion of the Golgi apparatus to the ER, and relocation of Golgi-resident proteins to the ER, suggesting profound effects of ARFA1C^{T31N} on ER function (Lee *et al.*, 2002). While overexpression of ARFA1E^{G69R} produced similar ER morphology in protoplasts, the organellar phenotype of 15A2 is distinct from ARFA1C^{T31N} overexpression. Alteration of ER morphology in 15A2 is relatively moderate, and Golgi-resident XYLT and KOR1 in the TGN and plasma membrane did not relocate to the ER, suggesting that the ER to Golgi transport was not blocked in the 15A2 line. On the other hand, in 15A2, there seems to be less separation between the Golgi apparatus and TGN, and endocytic recycling and endocytic transport were slower in 15A2, suggesting ARFA1E's roles in post-Golgi transport. In Fig. 6B, internalization of FM4-64 in 15A2 was not significantly slower than in the WT at the early time point, suggesting that the effect of ARFA1E^{G69R} is not at the level of the plasma membrane but at later steps of endocytic transport. This is consistent with the localization studies showing that WT ARFA1E mostly localizes in the Golgi apparatus/TGN compartment. However, during salt stress, ARFA1E^{G69R} caused retention of KOR1 at the plasma membrane, suggesting that ARFA1E^{G69R} could interfere with stress-induced endocytosis at the plasma membrane. It has been shown that multiple mechanisms operate during stress-induced endocytosis, and ARFA1E^{G69R} may be required for delivery and function of regulatory molecules (see below) at the plasma membrane.

The agglomerated structures in 15A2/ARFA1E^{G69R} contain the Golgi apparatus/TGN/EE. Since the prototypical function of ARFA1 is to promote formation of COPI- or COPII-coated vesicles in the ER and the Golgi apparatus, inhibition of ARFA1 function probably caused insufficient budding of vesicles in the ER and Golgi apparatus/TGN, resulting in accumulation of structures of mixed/intermediate characteristics. This applies to spherical ER structures because the phenotype of *elmo1* and *elmo2* mutants, which encode the ARF-GEF protein GNOM-LIKE and the COP-II coat protein SEC24a, respectively, important for promoting vesicle transport, mimics the ER phenotype of 15A2 (Nakano *et al.*, 2009). In Arabidopsis, two forms of TGN exist: the Golgi-associated TGN, which then dissociates from the Golgi apparatus to produce the Golgi-independent TGN, a proposed transit compartment for plasma membrane and secreted proteins (Uemura *et al.*, 2014, 2019). Dissociation of the TGN from the Golgi apparatus is inhibited by BFA, inducing formation of BFA bodies. In both BFA bodies and the agglomerated structures observed in the 15A2 cells, the Golgi apparatus and TGN became less distinct, suggesting that ARFA1E has an essential role in developing the TGN structure distinct from the Golgi apparatus. Notably, the *bex1*/ARFA1C^{L34F} mutant has been isolated based on enhanced BFA sensitivity (Tanaka *et al.*, 2014). BFA hypersensitivity of the *bex1*/ARFA1C^{L34F} mutation was genetically dominant, but ARFA1C^{L34F} can localize to the Golgi apparatus like WT ARFA1C. In addition, ARFA1C^{L34F} did not produce organellar agglomeration unless overexpressed via a heat shock protein promoter (Tanaka *et al.*, 2014). Indeed, the phenotype of *bex1/ARFA1C^{L34F}* was limited to the response to the treatment with BFA, which is a chemical that directly stabilizes the complex between ARF1 and ARF1-GDP exchange factor (GEF) (Zeeh *et al.*, 2006). It appears that the *bex1*/ARFA1C^{L34F} mutation specifically enhances BFA sensitivity of the ARF1C–GEF complex, causing dominant BFA sensitivity in seedlings. Unlike *bex1*/ARFA1C^{L34F}, ARFA1E^{G69R} alters organellar morphology and growth response in the absence of BFA, or additional mutations involved in ARF1 activation occur, reinforcing the significance of the ARFA1E^{G69R} allele. The relatively low expression level of the ARFA1C isoform may be partially responsible for the lack of phenotype in *bex1*/ARFA1C^{L34F} without BFA (Gebbie *et al.*, 2005). To date, the biochemical

bases of BFA hypersensitivity of *bex1*/ARFA1C^{L34F} have not been reported, but it was noted that the localization pattern of *bex1*/ARFA1C^{L34F} protein is similar to that of the constitutively active ARFA1C^{Q71L} mutant form (Tanaka *et al.*, 2014).

Several mechanisms that are not mutually exclusive may exist through which α-mannosidase I inhibition by KIF interacts with the ARFA1E mutation even though they operate in distinct subcellular compartments—inside and outside of endomembrane systems. It is unlikely that ARFA1 directly regulates the activity of glycoproteins (targets of KIF sensitivity) inside the secretory system. Rather, ARFA1 probably affects the delivery of glycoproteins to their site of action or affects turnover. Hence, one model assumes that incomplete *N*-glycan modification by ER mannosidases slows down the supply of *N*-glycoproteins, such as KOR1 and other proteins involved in cell wall polymer production. This may limit the biogenesis of cell wall polymers at the Golgi apparatus and the plasma membrane, which could be exacerbated by attenuation of endocytic recycling by the ARFA1E^{G69R} mutation. Previous studies reported that dysfunction of α-mannosidase I isoforms involved in *N*-glycan maturation causes a reduction in cell wall components, particularly pectin (Liebminger *et al.*, 2009). In fact, *mns1,2,3* triple knockout plants exhibited abnormally short and swollen roots, like cell wall-related mutants (Liebminger *et al.*, 2009), especially those that regularly cycle between the plasma membrane and TGN/EE and whose transient internalization is important for the establishment of salt tolerance, as shown for CesA and KOR1 (Endler *et al.*, 2015; Nagashima *et al.*, 2020a). Alternatively, it is also possible that the ARFA1-mediated process functions in parallel to the glycoprotein-mediated process in sustaining cell growth under mild stress (1× MS, 3% sucrose conditions). There are striking phenotypic similarities in the KIF response of 15A2, the salt response of *N*-glycosylation mutants, and plants overexpressing the mutated form of ARFA1C^{T31N} (Xu and Scheres, 2005). They all produce radially swollen root tips (including swollen epidermal cells) at cell division and in the elongation zone, often altering root hair morphology. Interestingly, ARFA1C^{T31N} can interfere with the proper localization of ROP2 (Xu and Scheres, 2005), a molecule that is essential for the microtubule-based salt tolerance mechanism (Shoji *et al.*, 2006; Wang *et al.*, 2007, 2011; Koiwa, 2009; Li *et al.*, 2017). Because the functions of the cellulose biosynthesis machinery, including KOR1 and the cellulose synthase complex, are mutually dependent on microtubule organization during normal growth and under stress (Baskin *et al.*, 2004; Paredez *et al.*, 2008; Kesten *et al.*, 2017), ARFA1E^{G69R} may interfere with ROP2-mediated microtubule reorganization under stress, enhancing the effect of salt or KIF.

Another possibility is that ARFA1E affects regulators of endomembrane systems. KOR1 and the cellulose synthase complex are transiently translocated from the plasma membrane to the TGN/endosome during salt stress (Endler *et al.*, 2015; Nagashima *et al.*, 2020a). As shown in Fig. 7C, the G69R mutation increased salt sensitivity in plants and interfered with the internalization of KOR1 under salt stress. A plasma membrane-locked form of KOR1 caused salt sensitivity in both *rsw2-1* and WT backgrounds, indicating that temporal internalization of KOR1 under salt stress is required for the salt adaptation process. This internalization of KOR1 was suppressed by 1-butanol, an inhibitor of phospholipase D1 (PLD1; Hu and Exton, 2005), and the phosphatidylinositol 4-kinase (PI4K) inhibitors phenylarsine oxide and wortmannin. In animal cells, PLD is involved in vesicle release from the plasma membrane, and ARF1 directly interacts with and activates PLDs (Brandenburg *et al.*, 2014). Also, Arabidopsis PLDζ2 is involved in the vesicular transport of PIN2 (Li and Xue, 2007), an auxin efflux carrier with a link to longitudinal root growth. ARF activation during salt stress may similarly help in translocating plasma membrane protein to the TGN. The importance of PI4K is seen in the salt stress-induced internalization of KOR1, the CesA3 internalization under sucrose-free growth conditions (Fujimoto *et al.*, 2015), and vacuolar targeting and degradation of aquaporin PIP2;1 (PLASMA MEMBRANE INTRINSIC PROTEIN2;1) during salt stress (Ueda *et al.*, 2016). In human cells, activation of PI4KIIIβ in the Golgi apparatus by protein kinase D requires ARF (reviewed in Graham and Burd, 2011), suggesting a possible role for ARFA1 in PI4K activation. Integration of these processes may occur at the plasma membrane by the protein kinase FERONIA (FER). FER interacts with pectic oligosaccharides and RALF (rapid alkalinization factor) peptides and is essential for regulating endocytosis (Liu *et al.*, 2024). Under stress conditions such as salt stress and heat stress, FER-mediated endocytosis is essential for tolerance and involves formation of biomolecular condensates and promiscus receptor clustering at the plasma membrane (Liu *et al.*, 2024). FER is required for maintain cell wall integrity (Feng *et al.*, 2018), and has been shown to function upstream of ROP2 and to form a complex with ROP2 in a guanine nucleotide-regulated manner (Duan *et al.*, 2010). Interestingly, overexpression of ARFA1C^{T31N} interferes with the delivery of the FER complex to the plasma membrane (Li *et al.*, 2015). It appears that ARFA1E and other ARFA1 family members have the potential for fine-tuning FER–ROP2 pathway outputs by mediating multiple inputs such as proper localization of FER–ROP2 and perhaps RALF ligands, cell wall polymer delivery, glycoprotein delivery for proper cellulose microfibril production, and microtubule organization. Current evidence only supports the passive role of ARFA1 in these processes; however, the activities of ARF-GEFs are phospho-regulated in animals (Walton *et al.*, 2020). Therefore, ARFA1 activation can be a part of a dynamic stress-specific membrane response involving protein kinases and PLD (Wang *et al.*, 2022; Dietz and Vogelsang, 2023).

Supplementary data

The following supplementary data are available at *JXB* online.

Fig. S1. Quantification of the confocal microscopic images.

Fig. S2. KIF sensitivity of mutant isolates.

Fig. S3. Salt sensitivity of the KIF-hypersensitive mutants.

Fig. S4. Features of *ARFA1E* and the mutant variants described in this study.

Fig. S5. GFP–KOR1 and BiP–*m*Cherry profiles in F_1 plants upon crossing.

Fig. S6. GFP–KOR1 and BiP–*m*Cherry profiles in *arfa1e-2*, with or without complementation.

Fig. S7. The G69R mutation did not cause the fusion of the Golgi apparatus/TGN to the ER.

Fig. S8. Normal morphology of the vacuole and the cell plate in 15A2.

Table S1. List of primer sequences used in this study

Acknowledgements

The authors thank the Arabidopsis Biological Resource Center (ABRC) for the provision of mutant stocks. We thank Drs Manoj K. Singh and Gerd Jürgens for providing the plasmid vectors used in the *in vitro* GDP–GTP exchange activity assay. We thank Ms Edith Torres, Abigale Roelke, and Khazina Amin for help with screening and mapping of the mutants.

Author contributions

YN and HK: designed the research; YN, VS, and L-FR: performed the experimental analyses; YN, L-FR, AvS, and HK: data analysis; YN and HK: wrote the manuscript, with editorial input by AvS.

Conflict of interest

The authors have no conflict of interest to declare.

Funding

This work was supported by the Mizutani Foundation [grant no. 220060] and the National Science Foundation [grant no. IOS-2049642] to HK, and the German Research Foundation [grant no. DFG 541/11-4] to AvS.

Data availability

All data supporting the findings of this study are available within the paper and within its supplementary data published online.

References

Baskin TI, Beemster GT, Judy-March JE, Marga F. 2004. Disorganization of cortical microtubules stimulates tangential expansion and reduces the uniformity of cellulose microfibril alignment among cells in the root of Arabidopsis. Plant Physiology **135**, 2279–2290.

Brandenburg LO, Pufe T, Koch T. 2014. Role of phospholipase D in G-protein coupled receptor function. Membranes (Basel) **4**, 302–318.

Colin L, Ruhnow F, Zhu JK, Zhao C, Zhao Y, Persson S. 2023. The cell biology of primary cell walls during salt stress. The Plant Cell **35**, 201–217.

Damm B, Schmidt R, Willmitzer L. 1989. Efficient transformation of *Arabidopsis thaliana* using direct gene transfer to protoplasts. Molecular & General Genetics **217**, 6–12.

Dietz KJ, Vogelsang L. 2023. A general concept of quantitative abiotic stress sensing. Trends in Plant Science **29**, 319–328.

Duan Q, Kita D, Li C, Cheung AY, Wu HM. 2010. FERONIA receptor-like kinase regulates RHO GTPase signaling of root hair development. Proceedings of the National Academy of Sciences, USA **107**, 17821–17826.

Elbein AD, Kerbacher JK, Schwartz CJ, Sprague EA. 1991. Kifunensine inhibits glycoprotein processing and the function of the modified LDL receptor in endothelial cells. Archives of Biochemistry and Biophysics **288**, 177–184.

Endler A, Kesten C, Schneider R, Zhang Y, Ivakov A, Froehlich A, Funke N, Persson S. 2015. A mechanism for sustained cellulose synthesis during salt stress. Cell **162**, 1353–1364.

Fagard M, Desnos T, Desprez T, Goubet F, Refregier G, Mouille G, McCann M, Rayon C, Vernhettes S, Hofte H. 2000. PROCUSTE1 encodes a cellulose synthase required for normal cell elongation specifically in roots and dark-grown hypocotyls of Arabidopsis. The Plant Cell **12**, 2409–2424.

Fan L, Li R, Pan J, Ding Z, Lin J. 2015. Endocytosis and its regulation in plants. Trends in Plant Science **20**, 388–397.

Fanata WI, Lee KH, Son BH, *et al*. 2013. N-glycan maturation is crucial for cytokinin-mediated development and cellulose synthesis in *Oryza sativa*. The Plant Journal **73**, 966–979.

Feng W, Kita D, Peaucelle A, *et al*. 2018. The FERONIA receptor kinase maintains cell-wall integrity during salt stress through Ca^{2+} signaling. Current Biology **28**, 666–675.e5.

Frank J, Kaulfurst-Soboll H, Rips S, Koiwa H, von Schaewen A. 2008. Comparative analyses of Arabidopsis *complex glycan1* mutants and genetic interaction with *staurosporin and temperature sensitive3a*. Plant Physiology **148**, 1354–1367.

Fujimoto M, Suda Y, Vernhettes S, Nakano A, Ueda T. 2015. Phosphatidylinositol 3-kinase and 4-kinase have distinct roles in intracellular trafficking of cellulose synthase complexes in *Arabidopsis thaliana*. Plant and Cell Physiology **56**, 287–298.

Gebbie LK, Burn JE, Hocart CH, Williamson RE. 2005. Genes encoding ADP-ribosylation factors in *Arabidopsis thaliana* L. Heyn.; genome analysis and antisense suppression. Journal of Experimental Botany **56**, 1079–1091.

Goldberg J. 1998. Structural basis for activation of ARF GTPase: mechanisms of guanine nucleotide exchange and GTP-myristoyl switching. Cell **95**, 237–248.

Graham TR, Burd CG. 2011. Coordination of Golgi functions by phosphatidylinositol 4-kinases. Trends in Cell Biology **21**, 113–121.

Hassler S, Lemke L, Jung B, Mohlmann T, Kruger F, Schumacher K, Espen L, Martinoia E, Neuhaus HE. 2012. Lack of the Golgi phosphate transporter PHT4;6 causes strong developmental defects, constitutively activated disease resistance mechanisms and altered intracellular phosphate compartmentation in Arabidopsis. The Plant Journal **72**, 732–744.

Hu T, Exton JH. 2005. 1-Butanol interferes with phospholipase D1 and protein kinase Calpha association and inhibits phospholipase D1 basal activity. Biochemical and Biophysical Research Communications **327**, 1047–1051.

Hüttner S, Veit C, Schoberer J, Grass J, Strasser R. 2012. Unraveling the function of *Arabidopsis thaliana* OS9 in the endoplasmic reticulum-associated degradation of glycoproteins. Plant Molecular Biology **79**, 21–33.

Hüttner S, Veit C, Vavra U, Schoberer J, Liebminger E, Maresch D, Grass J, Altmann F, March L, Strasser R. 2014. Arabidopsis class I α-mannosidases MNS4 and MNS5 are involved in endoplasmic reticulum-associated degradation of misfolded glycoproteins. The Plant Cell **26**, 1712–1728.

Jeong IS, Lee S, Bonkhofer F, *et al*. 2018. Purification and characterization of *Arabidopsis thaliana* oligosaccharyltransferase complexes from the native host: a protein super-expression system for structural studies. The Plant Journal **94**, 131–145.

Johnson KL, Jones BJ, Bacic A, Schultz CJ. 2003. The fasciclin-like arabinogalactan proteins of Arabidopsis. A multigene family of putative cell adhesion molecules. Plant Physiology **133**, 1911–1925.

Kang JS, Frank J, Kang CH, *et al*. 2008. Salt tolerance of *Arabidopsis thaliana* requires maturation of N-glycosylated proteins in the Golgi apparatus. Proceedings of the National Academy of Sciences, USA **105**, 5933–5938.

Kesten C, Menna A, Sanchez-Rodriguez C. 2017. Regulation of cellulose synthesis in response to stress. Current Opinion in Plant Biology **40**, 106–113.

Kim Y, Schumaker KS, Zhu JK. 2006. EMS mutagenesis of Arabidopsis. Methods in Molecular Biology **323**, 101–103.

Koiwa H. 2009. Pathways and genetic determinants for cell wall-based osmotic stress tolerance in the *Arabidopsis thaliana* root system. In: Jenks MA, Wood AJ, eds. Genes for plant abiotic stress. Chichester, UK: Wiley-Blackwell, 35–53.

Koiwa H, Li F, McCully MG, *et al*. 2003. The STT3a subunit isoform of the Arabidopsis oligosaccharyltransferase controls adaptive responses to salt/osmotic stress. The Plant Cell **15**, 2273–2284.

Lane DR, Wiedemeier A, Peng L, *et al*. 2001. Temperature-sensitive alleles of RSW2 link the KORRIGAN endo-1,4-beta-glucanase to cellulose synthesis and cytokinesis in Arabidopsis. Plant Physiology **126**, 278–288.

Lee MH, Min MK, Lee YJ, Jin JB, Shin DH, Kim DH, Lee KH, Hwang I. 2002. ADP-ribosylation factor 1 of Arabidopsis plays a critical role in intracellular trafficking and maintenance of endoplasmic reticulum morphology in Arabidopsis. Plant Physiology **129**, 1507–1520.

Lemière J, Ren Y, Berro J. 2021. Rapid adaptation of endocytosis, exocytosis, and eisosomes after an acute increase in membrane tension in yeast cells. eLife **10**, e62084.

Li C, Lu H, Li W, Yuan M, Fu Y. 2017. A ROP2–RIC1 pathway fine-tunes microtubule reorganization for salt tolerance in Arabidopsis. Plant, Cell & Environment **40**, 1127–1142.

Li C, Yeh F-L, Cheung AY, *et al*. 2015. Glycosylphosphatidylinositol-anchored proteins as chaperones and co-receptors for FERONIA receptor kinase signaling in Arabidopsis. eLife **4**, e06587.

Li G, Xue HW. 2007. Arabidopsis PLDzeta2 regulates vesicle trafficking and is required for auxin response. The Plant Cell **19**, 281–295.

Liebminger E, Huttner S, Vavra U, *et al*. 2009. Class I alpha-mannosidases are required for N-glycan processing and root development in *Arabidopsis thaliana*. The Plant Cell **21**, 3850–3867.

Linnenbrügger L, Doering L, Lansing H, Fischer K, Eirich J, Finkemeier I, von Schaewen A. 2022. Alternative splicing of Arabidopsis G6PD5 recruits NADPH-producing OPPP reactions to the endoplasmic reticulum. Frontiers in Plant Science **13**, 909624.

Liu M-CJ, Yeh F-LJ, Yvon R, Simpson K, Jordan S, Chambers J, Wu H-M, Cheung AY. 2024. Extracellular pectin–RALF phase separation mediates FERONIA global signaling function. Cell **187**, 312–330.e22.

López-Hernández T, Haucke V, Maritzen T. 2020. Endocytosis in the adaptation to cellular stress. Cell Stress **4**, 230–247.

Mansoori N, Timmers J, Desprez T, Kamei CL, Dees DC, Vincken JP, Visser RGF, Höfte H, Vernhettes S, Trindade LM. 2014. KORRIGAN1 interacts specifically with integral components of the cellulose synthase machinery. PLoS One **9**, e112387.

Mossessova E, Corpina RA, Goldberg J. 2003. Crystal structure of ARF1*Sec7 complexed with Brefeldin A and its implications for the guanine nucleotide exchange mechanism. Molecular Cell **12**, 1403–1411.

Murashige T, Skoog F. 1962. A revised medium for rapid growth and bio assays with tobacco tissue cultures. Physiologia Plantarum **15**, 473–497.

Nagashima Y, Ma Z, Liu X, Qian X, Zhang X, von Schaewen A, Koiwa H. 2020a. Multiple quality control mechanisms in the ER and TGN determine subcellular dynamics and salt-stress tolerance function of KORRIGAN1. The Plant Cell **32**, 470–485.

Nagashima Y, Ma Z, Zhang X, von Schaewen A, Koiwa H. 2020b. Lack of endoplasmic reticulum quality control (ERQC) promotes tonoplast (TP) targeting of KORRIGAN 1 (KOR1). Plant Signaling & Behavior **15**, 1744348.

Nagashima Y, von Schaewen A, Koiwa H. 2018. Function of N-glycosylation in plants. Plant Science **274**, 70–79.

Nakano RT, Matsushima R, Ueda H, Tamura K, Shimada T, Li L, Hayashi Y, Kondo M, Nishimura M, Hara-Nishimura I. 2009. GNOM-LIKE1/ERMO1 and SEC24a/ERMO2 are required for maintenance of endoplasmic reticulum morphology in *Arabidopsis thaliana*. The Plant Cell **21**, 3672–3685.

Naramoto S, Kleine-Vehn J, Robert S, *et al*. 2010. ADP-ribosylation factor machinery mediates endocytosis in plant cells. Proceedings of the National Academy of Sciences, USA **107**, 21890–21895.

Paez Valencia J, Goodman K, Otegui MS. 2016. Endocytosis and endosomal trafficking in plants. Annual Review of Plant Biology **67**, 309–335.

Paredez AR, Persson S, Ehrhardt DW, Somerville CR. 2008. Genetic evidence that cellulose synthase activity influences microtubule cortical array organization. Plant Physiology **147**, 1723–1734.

Pasqualato S, Renault L, Cherfils J. 2002. Arf, Arl, Arp and Sar proteins: a family of GTP-binding proteins with a structural device for 'front–back' communication. EMBO Reports **3**, 1035–1041.

Randazzo PA, Terui T, Sturch S, Fales HM, Ferrige AG, Kahn RA. 1995. The myristoylated amino terminus of ADP-ribosylation factor 1 is a phospholipid- and GTP-sensitive switch. Journal of Biological Chemistry **270**, 14809–14815.

Rips S, Bentley N, Jeong IS, Welch JL, von Schaewen A, Koiwa H. 2014. Multiple N-glycans cooperate in the subcellular targeting and functioning of Arabidopsis KORRIGAN1. The Plant Cell **26**, 3792–3808.

Robinson DG, Scheuring D, Naramoto S, Friml J. 2011. ARF1 localizes to the Golgi and the trans-Golgi network. The Plant Cell **23**, 846–849.

Roudier F, Fernandez AG, Fujita M, *et al*. 2005. COBRA, an Arabidopsis extracellular glycosyl-phosphatidyl inositol-anchored protein, specifically controls highly anisotropic expansion through its involvement in cellulose microfibril orientation. The Plant Cell **17**, 1749–1763.

Rui Q, Tan X, Liu F, Bao Y. 2022. An update on the key factors required for plant Golgi structure maintenance. Frontiers in Plant Science **13**, 933283.

Ryu KH, Huang L, Kang HM, Schiefelbein J. 2019. Single-cell RNA sequencing resolves molecular relationships among individual plant cells. Plant Physiology **179**, 1444–1456.

Schoberer J, König J, Veit C, Vavra U, Liebminger E, Botchway SW, Altmann F, Kriechbaumer V, Hawes C, Strasser R. 2019. A signal motif retains Arabidopsis ER-α-mannosidase I in the cis-Golgi and prevents enhanced glycoprotein ERAD. Nature Communications **10**, 3701.

Shi H, Kim Y, Guo Y, Stevenson B, Zhu JK. 2003. The Arabidopsis SOS5 locus encodes a putative cell surface adhesion protein and is required for normal cell expansion. The Plant Cell **15**, 19–32.

Shoji T, Suzuki K, Abe T, Kaneko Y, Shi H, Zhu JK, Rus A, Hasegawa PM, Hashimoto T. 2006. Salt stress affects cortical microtubule organization and helical growth in Arabidopsis. Plant and Cell Physiology **47**, 1158–1168.

Singh MK, Richter S, Beckmann H, *et al*. 2018. A single class of ARF GTPase activated by several pathway-specific ARF-GEFs regulates essential membrane traffic in Arabidopsis. PLoS Genetics **14**, e1007795.

Strasser R, Schoberer J, Jin C, Glössl J, Mach L, Steinkellner H. 2006. Molecular cloning and characterization of *Arabidopsis thaliana* Golgi α-mannosidase II, a key enzyme in the formation of complex N-glycans in plants. The Plant Journal **45**, 789–803.

Tanaka H, Nodzylski T, Kitakura S, Feraru MI, Sasabe M, Ishikawa T, Kleine-Vehn J, Kakimoto T, Friml J. 2014. BEX1/ARF1A1C is required for BFA-sensitive recycling of PIN auxin transporters and auxin-mediated development in Arabidopsis. Plant and Cell Physiology **55**, 737–749.

Ueda M, Tsutsumi N, Fujimoto M. 2016. Salt stress induces internalization of plasma membrane aquaporin into the vacuole in *Arabidopsis thaliana*. Biochemical and Biophysical Research Communications **474**, 742–746.

Uemura T, Nakano RT, Takagi J, *et al*. 2019. A Golgi-released subpopulation of the trans-Golgi network mediates protein secretion in Arabidopsis. Plant Physiology **179**, 519–532.

Uemura T, Suda Y, Ueda T, Nakano A. 2014. Dynamic behavior of the trans-Golgi network in root tissues of Arabidopsis revealed by super-resolution live imaging. Plant and Cell Physiology **55**, 694–703.

Vain T, Crowell EF, Timpano H, *et al*. 2014. The cellulase KORRIGAN is part of the cellulose synthase complex. Plant Physiology **165**, 1521–1532.

Veit C, Konig J, Altmann F, Strasser R. 2018. Processing of the terminal alpha-1,2-linked mannose residues from oligomannosidic N-glycans is critical for proper root growth. Frontiers in Plant Science **9**, 1807.

Vernoud V, Horton AC, Yang Z, Nielsen E. 2003. Analysis of the small GTPase gene superfamily of Arabidopsis. Plant Physiology **131**, 1191–1208.

Vikram M, Koiwa H. 2009. Glyphosate resistance as a versatile selection marker for Arabidopsis transformation. Plant Molecular Biology Reporter **27**, 132–138.

von Schaewen A, Sturm A, O'Neill J, Chrispeels MJ. 1993. Isolation of a mutant Arabidopsis plant that lacks N-acetyl glucosaminyl transferase I and is unable to synthesize Golgi-modified complex N-linked glycans. Plant Physiology **102**, 1109–1118.

Walton K, Leier A, Sztul E. 2020. Regulating the regulators: role of phosphorylation in modulating the function of the GBF1/BIG family of Sec7 ARF-GEFs. FEBS Letters **594**, 2213–2226.

Wang C, Li J, Yuan M. 2007. Salt tolerance requires cortical microtubule reorganization in Arabidopsis. Plant and Cell Physiology **48**, 1534–1547.

Wang C-F, Han G-L, Yang Z-R, Li Y-X, Wang B-S. 2022. Plant salinity sensors: current understanding and future directions. Frontiers in Plant Science **13**, 859224.

Wang S, Kurepa J, Hashimoto T, Smalle JA. 2011. Salt stress-induced disassembly of Arabidopsis cortical microtubule arrays involves 26S proteasome-dependent degradation of SPIRAL1. The Plant Cell **23**, 3412–3427.

Wu S-J, Ding L, Zhu J-K. 1996. *SOS1*, a genetic locus essential for salt tolerance and potassium acquisition. The Plant Cell **8**, 617–627.

Xia Y, Chu W, Qi Q, Xun L. 2015. New insights into the QuikChange process guide the use of Phusion DNA polymerase for site-directed mutagenesis. Nucleic Acids Research **43**, e12.

Xu J, Scheres B. 2005. Dissection of Arabidopsis ADP-RIBOSYLATION FACTOR 1 function in epidermal cell polarity. The Plant Cell **17**, 525–536.

Yorimitsu T, Sato K, Takeuchi M. 2014. Molecular mechanisms of Sar/Arf GTPases in vesicular trafficking in yeast and plants. Frontiers in Plant Science **5**, 411.

Zeeh JC, Zeghouf M, Grauffel C, Guibert B, Martin E, Dejaegere A, Cherfils J. 2006. Dual specificity of the interfacial inhibitor brefeldin A for Arf proteins and Sec7 domains. Journal of Biological Chemistry **281**, 11805–11814.

Zhu J, Gong Z, Zhang C, Song C-P, Damsz B, Inan G, Koiwa H, Zhu J-K, Hasegawa PM, Bressan RA. 2002. OSM1/SYP61: a syntaxin protein in Arabidopsis controls abscisic acid-mediated and non-abscisic acid-mediated responses to abiotic stress. The Plant Cell **14**, 3009–3028.